Provenance of the Neogene Deposits in the Western Himalayan Foreland Basin: Implications for Drainage Reorganization during the Late Miocene Uplift of the Himalaya

Akeek Maitra[1*], Robert Anczkiewicz[1], Szczepan J. Porębski[2], Dilip K Mukhopadhyay[3]

[1] Institute of Geological Sciences, Polish Academy of Sciences, Research Centre in Kraków, Kraków, Poland,

[2] Faculty of Geology, Geophysics and Environmental Protection, AGH University of Kraków, Poland,

[3] Department of Earth Sciences, Indian Institute of Technology Roorkee, India

Corresponding author: Akeek Maitra (akeek.maitra@ucalgary.ca)

[*]Current address: Department of Earth, Energy and Environment, Faculty of Science, University of Calgary, Alberta, Canada

Key Points:

- Siwalik Group rocks in western Himalayan foreland basin record Transhimalayan arc derived zircon as one of the major detrital components.
- The Transhimalayan magmatic arc was intermittently connected to the Himalayan foreland during slow Himalayan exhumation phases.
- Sutlej river acted as a transverse dispersal system that facilitated transport of arc detritus to the foreland basin across the Himalaya.

Abstract

Interaction between large-scale tectonics of the Himalaya and the Indian summer monsoon play a major role in shaping drainage systems of major Himalayan rivers. In this study we attempted to track the sediment sources of the Neogene–Quaternary fluvial deposits of the Kasauli Formation and Siwalik Group in the Subathu Basin of the Western Himalayan foreland basin. The depositional interval of these deposits spans from middle Miocene to Pliocene which overlap with the onset of Indian monsoon and its influence on the denudation of Himalayan rocks. Provenance analysis based on our detrital zircon U-Pb geochronology and bulk rock Sr-Nd-Hf isotope data indicates that these Neogene–Quaternary rocks record chiefly the exhumation of the Higher Himalayan Crystalline Sequence. However, at recurrent intervals within the Siwalik Group the presence of zircon population 40–110 Ma in age suggests a sediment sourcing from the Trans Himalayan batholith. We propose that the Sutlej River that originates in south Tibet acted as a transverse paleodispersal system and routed these arc-derived sediments to the Himalayan foreland basin via one of its extinct paleochannels. Zircon data suggest that this across-orogen routing system was particularly effective during the deposition of Middle Siwalik Formation (ca 11- 4.5 Ma), when the rate of uplift of the Himalaya decreased. On the other hand, the small-scale fluctuations in the presence of the Trans Himalayan zircons observed in the Lower and Upper Siwalik formations may primarily reflect climatic forcing, which induced changing monsoon precipitation and the Sutlej's transport capacity between dry and moist periods.

1 Introduction

Foreland basins are asymmetrical flexural depressions formed in front of an advancing orogenic load (Beaumont, 1981; Jordan, 1981). The principal characteristics of the foreland basins include (i) the location of the maximum subsidence and sediment thickness zone near the thrust load, (ii) sediment fill derived mostly from the rising orogen, and (iii) sediment recycling when the proximal fill itself becomes involved into basinward propagating thrust sheets and is available to erosion (DeCelles & Giles, 1996). Provenance studies of the foreland basin fills provide critical constraints for, among others, untangling orogen deformation and exhumation history, assessing the influence of hinterland and forebulge sediment sourcing, and discerning tectonically-driven events of river-drainage reorganization within source areas and the basin itself (Allen, 2017; Cawood et al., 2007; DeCelles et al., 1998; Eisbacher et al., 1974; Exnicios et al., 2022; Hirst & Nichols, 1986; Horton & Decelles, 2001; Koshnaw et al., 2017; Leonard et al., 2020; Vezzoli & Garzanti, 2009) The combination of rapid uplift of the Himalaya and high discharges intensified by monsoonal precipitation results in rapid erosion of the Himalayan bedrock (Bishop et al., 2002; Thiede et al., 2004; Grujic et al., 2006; Huntington et al., 2006). As a consequence, voluminous sediments are discharged through a large network of the Himalayan rivers into the adjoining foreland basin and distributed farther oceanwards as far as the Indus and Bengal fans to create the Earth's largest, modern source-to-sink sediment-dispersal systems (Blum et al., 2018; Clift et al., 2001). These sediments are delivered into the foreland basin through transverse dispersal from the rising orogenic wedge and via roundabout route by the Indus and Brahmaputra rivers, which bring clastic detritus from hinterland sources and enter the basin around the western and eastern Himalayan syntaxes, respectively (Figure 1). The Himalayan peripheral foreland basin originated in Early Paleocene times and since then, it accumulated a shallow-marine to continental sedimentary succession >8 km in thickness (Burbank et al., 1996).

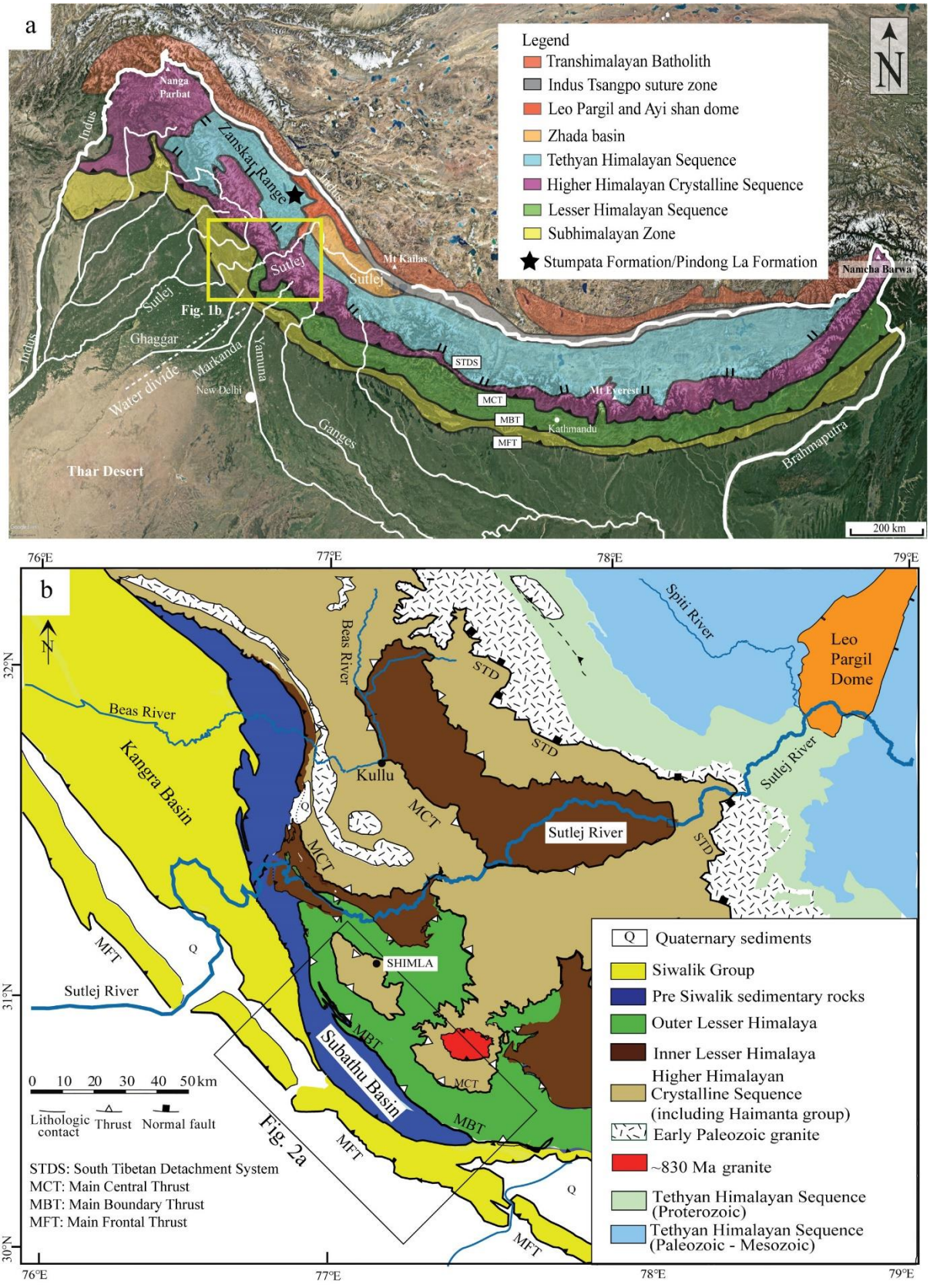
a
Legend
Transhimalayan Batholith
Indus Tsangpo suture zone
Leo Pargil and Ayi shan dome
Zhada basin
Tethyan Himalayan Sequence
Higher Himalayan Crystalline Sequence
Lesser Himalayan Sequence
Subhimalayan Zone
Stumpata Formation/Pindong La Formation
N
Nanga Parbat
Indus
Zanskar Range
Sutlej
Mt Kailas
Namcha Barwa
Fig. 1b
Ghaggar
Markanda
Yamuna
Water divide
New Delhi
STDS
MCT
MBT
MFT
Mt Everest
Kathmandu
Ganges
Brahmaputra
Thar Desert
200 km
b
76°E
77°E
78°E
79°E
32°N
31°N
30°N
Beas River
Kangra Basin
Kullu
Spiti River
Leo Pargil Dome
STD
Sutlej River
MCT
SHIMLA
MBT
Subathu Basin
MFT
Q
Fig. 2a
0 10 20 30 40 50 km
Lithologic contact
Thrust
Normal fault
STDS: South Tibetan Detachment System
MCT: Main Central Thrust
MBT: Main Boundary Thrust
MFT: Main Frontal Thrust
Quaternary sediments
Siwalik Group
Pre Siwalik sedimentary rocks
Outer Lesser Himalaya
Inner Lesser Himalaya
Higher Himalayan Crystalline Sequence (including Haimanta group)
Early Paleozoic granite
~830 Ma granite
Tethyan Himalayan Sequence (Proterozoic)
Tethyan Himalayan Sequence (Paleozoic - Mesozoic)

Figure 1. (**a**) Schematic diagram of the Himalaya showing main tectonic divisions and major drainage network of the Himalayan rivers (Le Fort, 1988). (**b**) Geological map of Himachal Pradesh (from Maitra et al., 2021). Rectangular box shows the study area (see Figure 2a).

The proximal, uplifted part of this succession is now exposed in the Sub-Himalaya zone and yielded a combined, orogenic and hinterland provenance signal based on U-Pb detrital zircon geochronology (Bracciali et al., 2015; Clift & Blusztajn, 2005; Govin et al., 2018; Jain et al., 2009; Najman, 2006; Wu et al., 2007; Zhuang et al., 2015). A notable exception is the Miocene Siwalik Group, which caps the foreland basin succession and lacks the evidence of a hinterland sourcing (Najman & Garzanti, 2000; Najman et al., 1997). This seems compatible with the alluvial-fan origin of the Siwalik Group (Dubille & Lavé, 2015; Parkash et al., 1980) and the existence of an orographic barrier between the foredeep and hinterland areas. However, the detrital zircon geochronology and Sr-Nd-Hf whole-rock isotope record from the Siwalik Group in the Subathu foreland (sub)basin of Himachal Pradesh, presented in this study, do carry a Trans-Himalaya signal enmixed with orogenic provenance fingerprints. We interpret this signal in terms of a changing drainage system driven by the Himalayan exhumation during the late Miocene–Pliocene.

2 Regional Geology

The Himalaya formed as a result of collision between India and Eurasia during the Paleocene. The boundary between the two continents is defined by the Indus-Tsangpo Suture Zone (ITSZ) composed of several thrust sheets containing Triassic–Eocene flysch deposits and Jurassic–Cretaceous ophiolitic mélanges derived from the subducted crust of the Neotethys Ocean (Burg & Chen, 1984). North of the suture, calc-alkaline plutons known as the Trans-Himalayan Batholith reflect magmatic activity associated with northward subduction of oceanic crust

beneath the southern margin of Eurasia. While throughout most of the orogen the pre-collisional magmatism took place in the Andean-type setting, in the NW part it was associated with the formation of the Kohistan-Ladakh intraoceanic arc (Bard, 1983; Khan et al., 1997; Reynolds et al., 1983). South of the suture, a series of highly deformed and variably metamorphosed nappes separated by the crustal scale, S-vergent discontinuities define the main tectonostratigraphic units of the Himalaya (Figure 1). Directly south of the suture, the Tethyan Himalaya Sequence (THS) comprises Neoproterozoic–Eocene metamorphosed and unmetamorphosed sediments that originated on the northern passive margin of the Indian continent. They are separated from the underlying Higher Himalaya Crystalline Sequence (HHCS) by a normal fault known as the South Tibetan Detachment System (STDS). The HHCS are formed predominantly by Proterozoic–early Paleozoic sediments with subordinate basic volcanic rocks metamorphosed under high grade conditions and subsequently intruded by leucogranites. The Main Central Thrust (MCT) divides them from the structurally lower Lesser Himalaya Sequence (LHS) locally sub-divided into the Inner Lesser Himalaya (ILH) and Outer Lesser Himalaya (OLH). The ILH crops out in several tectonic windows within the HHCS and represents the Paleoproterozoic sediments of low to medium metamorphic grade (Figure 1). The OLH comprises a Neo-Proterozoic to Cambrian, typically, low-grade metasediments emplaced over the foreland basin along the Main Boundary Thrust (MBT).

The foreland basin, commonly referred to as the Sub-Himalaya, comprises Cenozoic marine and continental deposits thrust over the Indo-Gangetic Plain along the Main Frontal Thrust (MFT), the youngest major Himalayan discontinuity (Figure 1). In the Himachal Pradesh region of NW India, the Himalayan foreland succession is broadly similar to that in other Sub Himalayan regions (see overviews in Garzanti, 2019; Najman, 2006; Yin, 2006). It crops out in the Subathu Basin (Figure 2a) that is divided into the Kangra and Subathu sub-basins (Figure 1b).

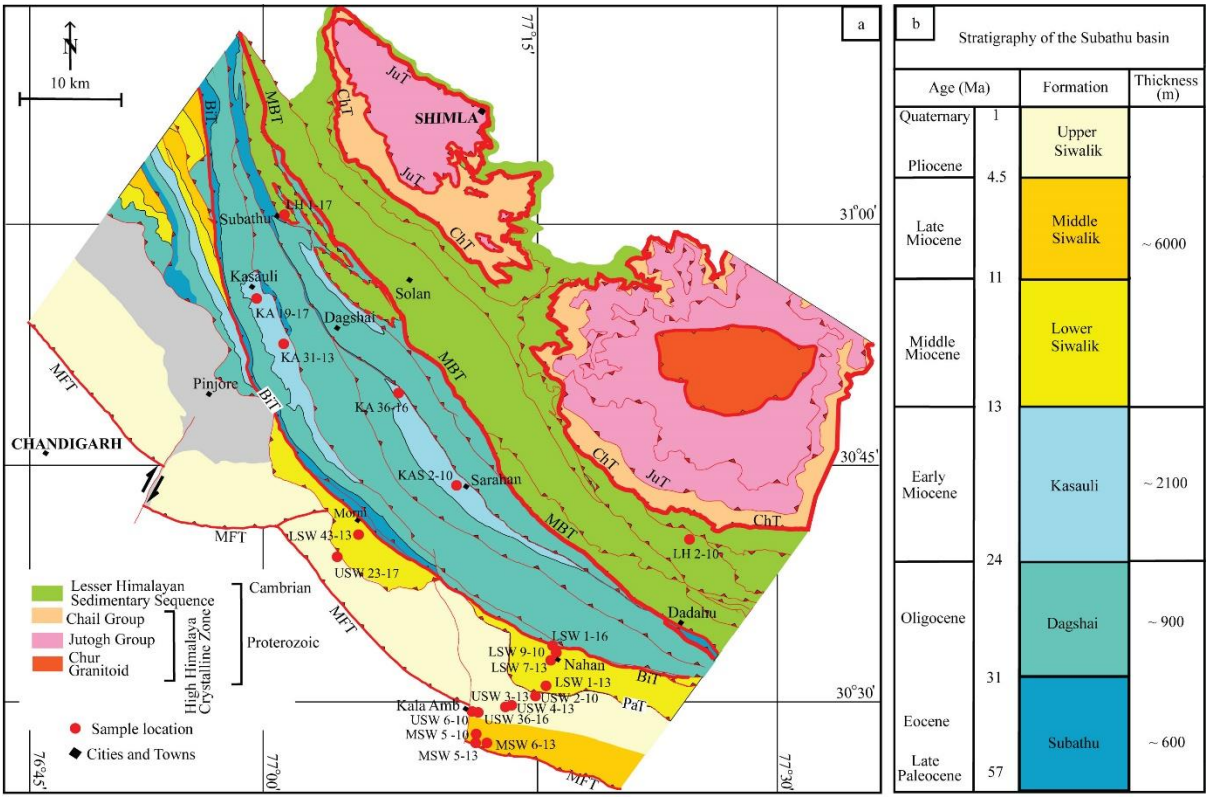

Figure 2. (**a**) Geological map of the Subathu Basin of Himachal Pradesh with sample location of U-Pb ages and whole rock isotopes. Map modified after Khan and Prasad (1998), Mishra and Mukhopadhyay (2012), Philip et al. (2012), and Pilgrim and West (1928). (**b**) Stratigraphy of the Cenozoic succession of the Subathu Basin.

The succession begins with the Paleocene–Eocene Subathu Formation, which consists of black and red mudstones interbedded with sandstones, oyster-bearing limestones and bedded gypsum. These sediments are thought to have originated on a shoaling-upward shelf (Bera et al., 2010). The overlying Oligocene Dagshai Formation consists of fluvial channel sandstones, overbank mudstones and numerous red paleosoil (Figure 2b) (Bera et al., 2008; Najman et al., 2004). The contact between these two formations is commonly accepted as an erosional unconformity. However, the span of erosional hiatus and even the mere presence of the unconformity are still debated (Bera et al., 2008; Bhatia & Bhargava, 2006; Najman et al., 2004; Singh, 2010). The Dagshai Formation grades conformably upwards into the Kasauli Formation, which consists of greenish grey, micaceous, cross-bedded sandstones interlayered

144 locally by mudstones and siltstones (Singh, 1978). These sediments represent braided-river
145 alluvium (Najman et al., 2004; Singh, 1978). Due to paucity of geochronological data, the onset
146 of deposition of the Kasauli Formation is uncertain but it is approximated as the early Miocene
147 (Arya et al., 2004, 2001; Arya & Awasthi, 1994; Awasthi et al., 1994). Based on
148 biostratigraphic and thermochronological data the boundary between the Dagshai and Kasauli
149 formations could be ascertained at 24 Ma (Arya et al., 2004, 2001; Arya & Awasthi, 1994; Jain
150 et al., 2009; Najman et al., 1997; Srivastava et al., 2014).

151 The Neogene Siwalik Group is the thickest (~ 6000 m) among all the lithostratigraphic units
152 of the Subathu Basin infill. It conformably overlies the Kasauli Formation, and is subdivided
153 into the Lower, Middle and Upper Siwalik formations (Pilgrim, 1910). This tripartite division
154 can be observed along the entire strike of the entire Himalaya, although the age boundaries
155 between these three formations vary. The Siwalik Group consists of immature sandstones,
156 conglomerates and fine-grained intercalations. These lithologies are arranged into two, large-
157 scale coarsening-upward successions, which reflect deposition within stream-dominated,
158 piedmont megafans merging distally into alluvial plain dominated by axial dispersal (Parkash
159 et al., 1980; Tandon, 1991). The boundary between the Kasauli Formation and the Lower
160 Siwalik Formation is assumed to fall at ~13 Ma (White et al., 2001). Biostratigraphic evidence
161 indicates that the boundary between the Lower and Middle Siwalik formations is 11 Ma in age,
162 whereas that between the Middle and Upper Siwalik falls at 4.5 Ma (Meigs et al., 1995; Pillans
163 et al., 2005; Sehgal & Bhandari, 2014). The upper age boundary of the Upper Siwalik
164 Formation is ~1 Ma (Brozovic & Burbank, 2000; Meigs et al., 1995; Nanda, 2002; Patnaik,
165 2003; Rao et al., 1995; Kumar et al., 2019). The entire foreland basin underwent intense
166 shortening expressed as a series of small-scale nappes bounded by the SW-verging thrusts
167 (Powers et al., 1998; Srivastava & Mitra, 1994).

168

3 Samples and Methods

Sample locations are marked on a geological map in Figure 2a and the GPS coordinates of each location are given in supporting information Table S1. Four samples represent the Kasauli Formation and the remaining samples belong to the Siwalik Group. Majority of Siwalik samples were collected in the Kala–Amb–Nahan region, with the exception of two samples taken near the town of Morni, about 20 km NW of Nahan (Figure 2a).

About 3–5 kilogram of a sample was crushed down to a fraction < 315 µm. A representative split (c. 100 g) was milled to powder and subsequently used for bulk rock geochemistry and Sr-Nd-Hf isotopic analyses. Zircons were extracted using commonly used techniques of magnetic and heavy liquid separation followed by hand-picking under the stereo-microscope. Subsequently they were mounted in an epoxy resin and polished using diamond pastes. U-Pb geochronology and Sr-Nd-Hf isotopic analyses were carried out in Kraków Research Centre, Institute of Geological Sciences, Polish Academy of Sciences. Laser ablation ICP-MS U-Pb zircon dating was conducted using an excimer laser (ArF) RESOlution by Resonetics (now Applied Spectra) equipped with double volume S155 Laurine Technic sample cell. The laser was coupled with XseriesII quadrupole ICP-MS by ThermoFisher Scientific. Analytical protocols follow the approach described in Anczkiewicz & Anczkiewicz (2016). The main instrument parameters applied during the measurements are summarized in supporting information Table S2. Data reduction and age calculations were performed using Iolite 3 (Paton et al., 2011). Zircon Z91500 was used as a primary standard and the quality of the results was monitored by frequent measurements of zircons GJ1 (Jackson et al., 2004) and Plešovice (Sláma et al., 2008). Over the course of analyses the concordia ages of the secondary standards were accurate within ≤ 1% precision during each analytical session. About 80–110 crystals (depending on zircon availability) were analyzed per sample. The detrital zircon age distributions are represented as kernel density estimate (KDE) plots with a bandwidth of 30

(Figure 3a). Ages with more than 10% discordance were excluded from the KDE plots. In the case of ages > 1 Ga, $^{207}Pb/^{206}Pb$ ages were used. The KDE spectra along with the pie diagrams were plotted using DetritalPy v1.1 package (Sharman et al., 2018).

Isotopic compositions of Sr and Nd were measured for all the eighteen samples analyzed for U-Pb zircon geochronology. Hafnium isotopic ratios were measured for the same samples except for KAS 2-10, USW 2-10, MSW 5-10, USW 6-10 and LSW 9-10. Sample digestion and ion column chemistry were carried out following the procedures described in Anczkiewicz & Anczkiewicz (2016) and Anczkiewicz et al. (2004). Isotope ratio measurements were performed using Neptune multicollector inductively coupled plasma mass spectrometer (MC-ICP-MS) in static mode. Reproducibility of Sr, Nd and Hf isotopic composition of standards measured over the course of analyses is given in a caption to Table 1. Variations in Nd and Hf isotopic composition were expressed as εNd_0 and εHf_0 calculated relatively to the present-day CHUR reservoir with the reference ratios $^{143}Nd/^{144}Nd_{CHUR} = 0.512638$, $^{147}Sm/^{144}Nd_{CHUR} = 0.0197$ (Jacobsen & Wasserburg, 1980) and $^{176}Hf/^{177}Hf_{CHUR} = 0.282785$ and $^{176}Lu/^{177}Hf_{CHUR} = 0.0336$ (Bouvier et al., 2008).

4 Results

4.1 U-Pb Geochronology

The U-Pb detrital zircon dating results are summarized in supporting information Table S1 and graphically presented as KDE plots in Figure 3a. The samples are arranged from the oldest at the bottom to the youngest on the top of the figure. Although no high-resolution stratigraphic data are available, the relative time of deposition can be established for all the studied strata in the Kala Amb – Nahan section, which exposes a NE-dipping homocline. Two additional samples from the Upper and Lower Siwalik strata near Morni were inserted into the

stratigraphic order on the basis of the similarity of the zircon age distribution patterns with the samples in the main studied section (Figure 3a).

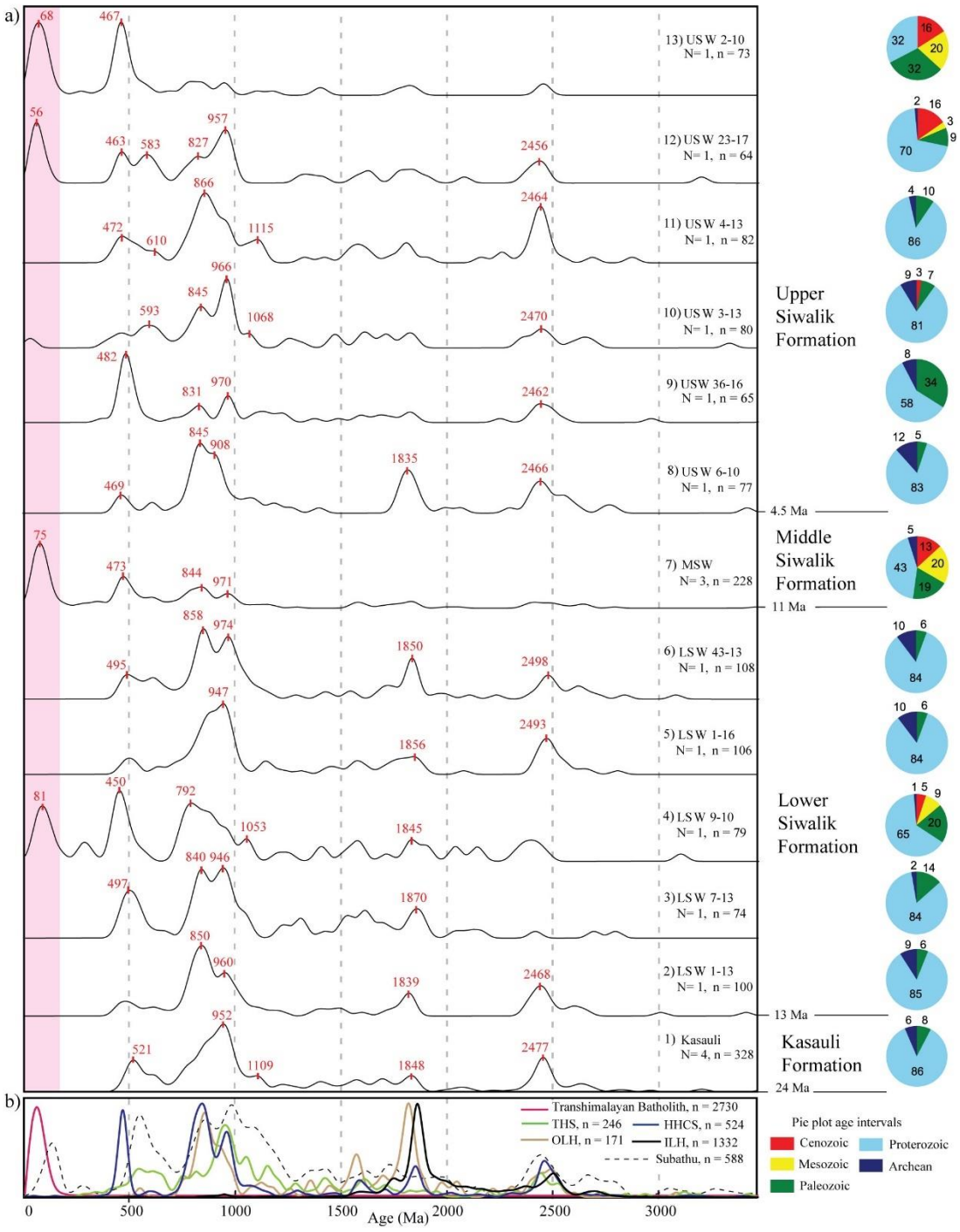

Figure 3. (**a**) Kernel density estimates of the samples taken from the Kasauli Formation and Siwalik Group. A 30-Ma bandwidth is assumed for all samples and reference spectrum of the Himalayan

sources. Composite zircon spectra are given for the Kasauli Formation and Middle Siwalik Formation (MSW) where *N* denotes the number of samples combined into the composite spectra and *n* denotes number of grains analysed. The red numbers show major peaks of each KDE. Pie plots in the right panel show the proportional distribution of the detrital zircon population. (**b**) Compilations of zircon spectra for Himalayan sources from Himachal Pradesh. Data sources: HHC – Cawood et al. (2007), Mandal et al. (2015), Spencer et al. (2012), Webb et al. (2011); THS – Myrow et al. (2010); ILH – Gehrels et al. (2011); OLH – this study; Subathu Formation – Colleps et al. (2020, 2019), Ravikant et al., (2011);Transhimalayan sources – Bosch et al. (2011), Bouilhol et al., (2013), DeCelles et al., (2011), Jagoutz et al., (2009), Krol et al., (1996), Ravikant et al., (2009), Schärer et al., (1984), Singh et al., (2007), St-Onge et al., (2010), Upadhyay et al., (2008), Wang et al., (2012), White et al., (2011) and Zhang et al., (2011).

In order to constrain the provenance of Kasauli and Siwalik sediments, we constructed KDE age spectra of the most probable source regions represented by the Himalayan and Trans Himalayan domains (Figure 3a, b). The reference spectra for the HHCS, ILH and THS were compiled using data available for the Indian NW Himalaya (Cawood et al., 2007; Gehrels et al., 2011; Mandal et al., 2015; Myrow et al., 2010; Spencer et al., 2012; Webb et al., 2011) and our own data in the case of the OLH (Figure S1). For the Subathu Formation, we used data from Colleps et al. (2020, 2019) and Ravikant et al. (2011). The ages of the magmatic events reported for the Trans Himalayan Batholith were compiled from Bosch et al. (2011), Bouilhol et al. (2013), DeCelles et al. (2011), Jagoutz et al. (2009), Krol et al. (1996), Ravikant et al. (2009), Schärer et al. (1984), Singh et al. (2007), St-Onge et al. (2010), Upadhyay et al. (2008), Wang et al. (2012), White et al. (2011), and Zhang et al. (2011). Although the number of studies in the NW Himalaya is limited, we find this approach more appropriate than relying on the larger dataset produced for the distant region of the central Himalaya (Gehrels et al., 2011). Comparison of both regions (presented in supporting information Figure S1) reveals some significant differences particularly well visible for the Higher Himalaya where sharp Neoproterozoic zircon peaks are practically absent in the Central Himalaya. Some smaller shifts and differences in zircon proportions are also detectable in the other main tectonic units. Below we characterize changes in zircon age components in the Neogene sandstones of the Subathu Basin.

253 The oldest, Archaean zircons in the studied rocks are scarce at the order of several percent but
254 reach 12% in sample USW 6-10 (Figure 3a:8). The Proterozoic zircons dominate in nearly all
255 samples and constitute from 43 to 86%. The only exception is the Upper Siwalik sample USW
256 2-10 where the Proterozoic zircons content is as low as 32%. The Paleo- and Meso-Proterozoic
257 zircons are spread throughout the KDE spectra and form two distinct peaks at about 2.5 and
258 1.8 Ga that can be traced in the vast majority of the samples. The 2.5 Ga peak is weak or absent
259 in LSW 7-13 and in all Middle Siwalik samples. The 1.8 Ga peak is absent in the Middle
260 Siwalik deposits and very weak in the majority of the Upper Siwalik sandstones with the
261 exception of sample USW 6-10, where it is one of the major age components. The Late
262 Mesoproterozoic and younger zircons form a much more variable age patterns that we describe
263 below.

264 Analyses of 4 samples representing the Kasauli Formation (KA 19-17, KA 33-16, KA 31-13
265 and KAS 2-10) showed no resolvable differences and hence were compiled into a single KDE
266 plot. The cumulative zircon age spectrum shows dominant age groups between 400 and 600
267 Ma with a 520 Ma peak, and between 700 and 1100 Ma with a 950 Ma peak. In the latter group
268 there is also a weak signal of 1.1 Ga zircons (Figure 3a:1).

269 The Siwalik Group shows significant differences among the KDE age spectra. The Lower
270 Siwalik zircon age distributions are generally similar to the patterns observed for the Kasauli
271 Formation with the major difference confined to the presence of an additional peak at 850 Ma
272 in samples LSW 1-13, LSW 7-13, LSW 43-13 (Figure 3a:2, 3, 6). Moreover, the amount of
273 450–500 Ma zircons varies throughout the Lower Siwalik from minor in LSW 1-13 and LSW
274 1-16 to substantial in LSW 9-10 (Figure 3a:2–6). The latter sample is unique among the Lower
275 Siwalik deposits due to the presence of the Late Cretaceous zircons defining about 80 Ma peak
276 and due to the presence of ~1.1 Ga zircon grains (Figure 3a:4).

277 The three Middle Siwalik samples are internally very consistent and were compiled into a
278 single KDE plot (Figure 3a:7). In contrast to the older strata, they contain much smaller
279 amounts of 700–1000 Ma and 400–600 Ma zircons. The age spectrum is dominated by the
280 Cretaceous peak of about 75 Ma.

281 The Upper Siwalik Formation shows KDEs similar to the Lower Siwalik sample LSW 43-13.
282 In comparison to older samples, typically, the Upper Siwalik sediments do not contain a
283 significant amount of 1.8 Ga zircons. The only exception is USW 6-10, where this peak belongs
284 to the second most abundant in the zircon age population (Figure 3a:8). Proceeding towards
285 younger strata (Figure 3a:9–12), we observe changes in relative proportion of the two major
286 zircon populations (400–600 Ma and 700–1000 Ma). In two samples, there is a major
287 participation of the young Cretaceous zircons. In the youngest sandstone (USW 2-10), the
288 Cretaceous and Early Ordovician zircons dominate the whole spectrum. The 700–1000 Ma
289 peak, on the other hand, nearly disappears. The latter sample strongly resembles those of the
290 Middle Siwalik Formation (Figure 3a:13).

291 4.2 Whole Rock Sr-Nd-Hf Isotopic Geochemistry

292 Whole rock Sr-Nd-Hf isotopic data are summarized in Table 1 and isotope ratio plots are shown
293 in supporting information Figure S2. The Kasauli Formation samples show a relatively narrow
294 range of $^{87}Sr/^{86}Sr$ ratios (0.751317 to 0.755084) accompanied by a fairly large spread in
295 $^{87}Rb/^{86}Sr$ ratios ranging from 2.9 to 5.7 (Figure S2a). The Siwalik Group deposits show a larger
296 variability (Figure S2a). Most of the samples form a linear array with a few “outliers” on the
297 Rb-Sr diagram (Figure S2a). Strontium isotopic ratios of the Lower Siwalik Formation range
298 between 0.719099 and 0.766187.

299

Sample	Th/Sc	Rb [ppm]	Sr [ppm]	$^{87}Rb/^{86}Sr$	$^{87}Sr/^{86}Sr$	2 s.e	Sm [ppm]	Nd [ppm]	$^{147}Sm/^{144}Nd$	$^{143}Nd/^{144}Nd$	2 s.e	εNd_0	Lu [ppm]	Hf [ppm]	$^{176}Lu/^{177}Hf$	$^{176}Hf/^{177}Hf$	2 s.e	εHf_0
KA 19-17	1.82	60.3	48.20	3.6354	0.752525	0.000014	4.56	24.5	0.1125	0.511904	0.000005	-14.3	0.33	4.1	0.011	0.282330	0.000005	-16.1
KA 31-13	1.50	60.5	60.60	2.9010	0.751923	0.000012	4.1	21.9	0.1131	0.511898	0.000006	-14.4	0.4	4	0.014	0.282283	0.000004	-17.7
KA 33-16	1.63	56.3	42.30	3.8673	0.751317	0.000012	4.9	26.8	0.1105	0.511898	0.000004	-14.4	0.29	3.9	0.011	0.282302	0.000005	-17.1
KAS 2-10	1.93	61	31.20	5.6829	0.755084	0.000010	4.89	25.9	0.1141	0.511876	0.000015	-14.9	-	-		-	-	-
LSW 1-13	1.48	57.4	36.40	4.5816	0.750582	0.000012	3.73	19.5	0.1156	0.511843	0.000006	-15.5	0.28	4	0.010	0.282242	0.000004	-19.2
LSW 1-16	1.62	47.9	19.80	7.0318	0.755143	0.000011	4.32	21.4	0.1220	0.511871	0.000006	-15.0	0.26	3.9	0.010	0.282226	0.000005	-19.8
LSW 43-13	1.65	58.3	24.10	7.0391	0.766187	0.000012	3.86	20.8	0.1121	0.511829	0.000006	-15.8	0.31	5.1	0.009	0.282154	0.000006	-22.3
LSW 7-13	2.16	89.1	35.60	7.2810	0.763758	0.000011	5.72	31	0.1115	0.511817	0.000005	-16.0	0.38	8.9	0.006	0.282132	0.000006	-23.1
LSW 9-10	0.93	53.2	143.60	1.0731	0.719099	0.000012	4.53	23.9	0.1145	0.512060	0.000007	-11.3	-	-	-	-	-	-
MSW 5-13	0.97	71.6	137.40	1.5100	0.723234	0.000010	3.94	18.7	0.1273	0.512047	0.000005	-11.5	0.27	3	0.013	0.282443	0.000004	-12.1
MSW 6-13	1.05	53.8	180.20	0.8645	0.716359	0.000009	5.99	32.5	0.1114	0.512162	0.000005	-9.3	0.45	6.5	0.010	0.282459	0.000004	-11.5
MSW 5-10	1.10	45.4	212.80	0.6178	0.716043	0.000011	3.89	21.6	0.1088	0.512106	0.000012	-10.4	-	-	-	-	-	-
USW 6-10	2.37	58.2	71.60	2.3636	0.759001	0.000015	5.21	27.2	0.1157	0.511729	0.000008	-17.7	-	-	-	-	-	-
USW 3-13	2.70	36.3	18.70	5.6442	0.758382	0.000011	3.28	17.8	0.1113	0.511837	0.000006	-15.6	0.25	7.2	0.005	0.282051	0.000004	-26.0
USW 36-16	2.88	72	70.40	2.9718	0.751898	0.000011	4.43	23.6	0.1134	0.511862	0.000006	-15.1	0.3	6.1	0.007	0.282177	0.000007	-21.5
USW 4-13	1.53	40.5	22.90	5.1403	0.754423	0.000009	2.99	15.7	0.1151	0.511875	0.000007	-14.9	0.22	3.3	0.010	0.282209	0.000004	-20.4
USW 23-17	0.94	40.4	119.00	0.9832	0.718010	0.000016	2.27	11.9	0.1153	0.512180	0.000005	-8.9	0.16	1.8	0.013	0.282444	0.000005	-12.0
USW 2-10	1.28	75.9	88.70	2.4806	0.727683	0.000013	4.14	23.7	0.1055	0.512007	0.000021	-12.3	-	-	-	-	-	-

Table 1. Whole rock Sr-Nd-Hf ratios of Kasauli Formation and Siwalik Group samples. Uncertainties are expressed as 2SD (standard deviations). Reproducibility of isotope ratios of Sr standard (SRM987) $^{87}Sr/^{86}Sr = 0.710265 \pm 0.000009$ (n = 6); Nd standard (JdNd-1) $^{143}Nd/^{144}Nd = 0.512103 \pm 0.000007$ (n=5) and Hf standard (JMC475) $^{176}Hf/^{177}Hf = 0.282156 \pm 0.000005$ (n=7) was achieved over a course of analyses. $^{143}Nd/^{144}NdCHUR_0 = 0.512638$ and $^{147}Sm/^{144}NdCHUR_0 = 0.0197$ (Hamilton et al., 1983; Jacobsen & Wasserburg, 1980); $^{176}Hf/^{177}HfCHUR_0 = 0.282785$ and $^{176}Lu/^{177}Hf$ $CHUR_0 = 0.0336$ (Bouvier et al., 2008). Decay constant $\lambda^{147}Sm = 6.54 \times 10{-}12$ yr−1 (Lugmair & Marti, 1978). Decay constant $\lambda^{176}Lu = 1.865 \times 10{-}11$ yr−1 adopted from Scherer et al. (2001).

All three Middle Siwalik samples show less radiogenic $^{87}Sr/^{86}Sr$ values (0.716043–0.723234) and the Upper Siwalik rocks are again more radiogenic (0.718010–0.759001). In general, high $^{87}Sr/^{86}Sr$ ratios are accompanied by high $^{87}Rb/^{86}Sr$ ratios.

Isotopic compositions of Nd and Hf of the Kasauli sandstones show limited variations with $^{143}Nd/^{144}Nd$ ratios between 0.511876–0.511904 and $^{176}Hf/^{177}Hf$ ratios between 0.282283 and 0.282330. The Siwalik Group samples show broader variations, and in the case of Nd isotopes, tend to be more radiogenic. Higher $^{143}Nd/^{144}Nd$ ratios do not correlate with $^{147}Sm/^{144}Nd$ (Figure S2b). In the case of Hf isotopes, the Siwalik Group samples show a broader range of ratios, but their values tend to positively correlate with the $^{176}Lu/^{177}Hf$ ratios. The largest Nd-Hf isotopic variations are observed for the Upper Siwalik samples. The $^{143}Nd/^{144}Nd$ values range from 0.511729 to 0.512180 and $^{176}Hf/^{177}Hf$ ratios range from 0.282051 and 0.282444. Isotopic composition of all the remaining samples falls within these ranges (Figure S2 b, c).

4.3 Multidimensional Scaling

We used multidimensional scaling (MDS) as a statistical accessory to U-Pb detrital zircon geochronology (Vermeesch, 2013; Vermeesch & Garzanti, 2015). Figure 4 illustrates the degree of similarity of the sample age distribution patterns. The smaller the distance between the samples the higher the degree of similarity. The plot was created using DetritalPy v. 1.1 package (Sharman et al., 2018), where Kolmogorov-Smirnov (K-S) distance measurement (D_{max}) was chosen as dissimilarity measurement criterion (Vermeesch, 2013, 2018). Together with the samples, we plotted the reference KDE spectra constructed for the most probable source regions. The Kasauli and Lower Siwalik samples group into one cluster denoting close resemblance. Three samples from the Middle Siwalik and one from the Upper Siwalik

Formation plot away from this cluster due to the presence of the Mesozoic and Cenozoic zircons, absent in the main cluster.

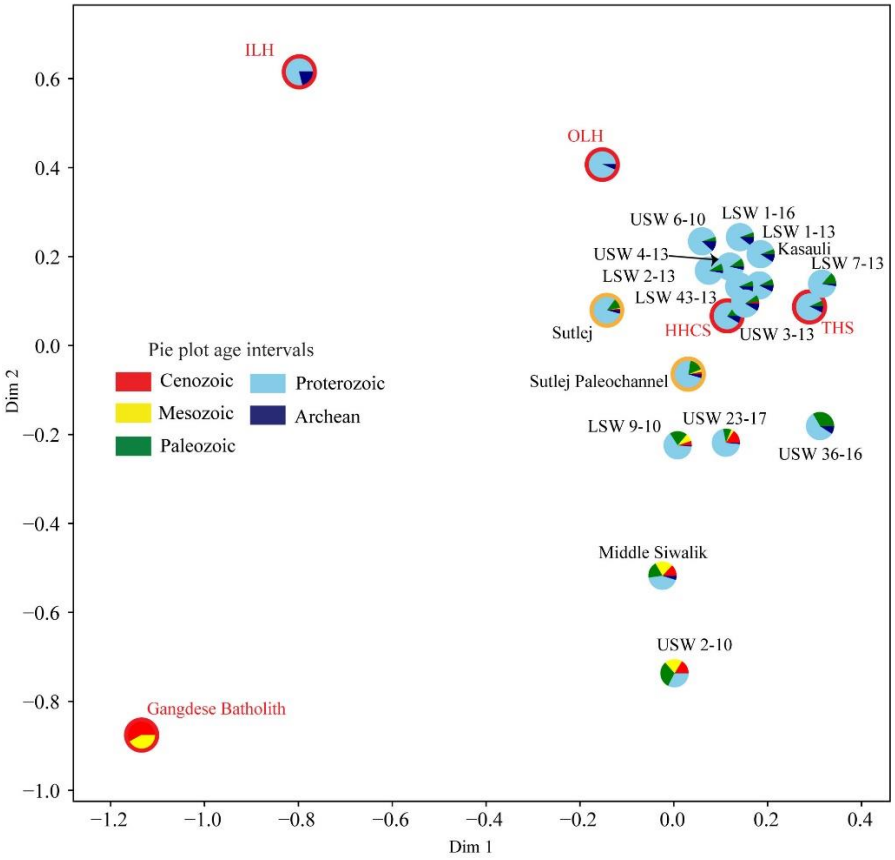

Figure 4 MDS plot of the Kasauli Formation and the Siwalik Group samples analysed for U-Pb detrital zircon geochronology. Each sample is shown as pie of the constituent ages of the zircon population. For comparison, the Himalayan sources and Gangdese Batholith are shown in red circles and modern sediments of the Sutlej River are shown in orange circles.

5 Discussion

5.1 U-Pb Detrital Zircon Ages

The KDE plot of the detrital zircon ages from the Kasauli Formation resembles age distribution patterns of the THS and the HHCS (Figure 3b). The KDEs of these two potential source regions show considerable overlap but can be distinguished based on the maxima in the 400–600 Ma age interval. While the THS zircons show a very broad peak between 530 and 650 Ma, the HHCS show a narrow peak at 470 Ma. Moreover, zircon ages between 750 and 1200 Ma show

bimodal distribution in the HHCS with peaks at ~850 and 970 Ma, whereas the THS have a prominent, single peak at about 960 Ma in the same age range (Figure 3b). The lack of bimodal distribution between 750 and 1200 Ma and the presence of the ~520 Ma peak suggest the THS as a dominant source of the detritus in the Kasauli Formation. On the other hand, the presence of a small 1.8 Ga peak points to some contribution from the HHCS region.

The Lower Siwalik samples show variable KDE spectra, but the majority show all peaks characteristic of the HHCS (Figure 3a, b). An important exception is sample LSW 9-10, which reveals a very distinct group of young zircons defining the 81 Ma peak (Figure 3a:4). The presence of the Cretaceous–Eocene zircons suggests sediment transport across the Himalayan range from the Trans Himalayan Batholith, where such zircons are abundant. Alternatively, the young zircons could have been incorporated into the Siwalik Group by reworking of the Subathu Formation. Colleps et al. (2020) report the KDE detrital zircon ages for the Subathu Formation from our study area, whose distribution shows large degree of similarity with the KDE plot obtained for the Lower Siwalik Formation in this study (Figure 3). However, Subathu sediments display a distinct, broad ~1 Ga peak and a very distinct peak of ~540 Ma. Both peaks are absent in the LSW 9-10 sample. Thus, although some recycling of Subathu sediments into the younger basin fill cannot be ruled out, we prefer to link the presence of young zircons primarily with the Trans Himalayan Batholith source. The Cretaceous–Cenozoic zircons with a peak of about 75 Ma dominate all Middle Siwalik samples (Figure 3a:7). Unlike the LSW9-10 sample, here the KDE spectra do not resemble the Subathu Formation zircon-age pattern and point unequivocally to the Trans Himalayan Batholith as the main source of the detritus. The subordinate contribution from the Indian crust is marked by the presence of ~480 Ma zircons likely derived from the Ordovician granitoids intruding basement rocks.

The Upper Siwalik KDE plots are very similar to those of the Lower Siwalik deposits described above. Some variations in peak intensities are observed, particularly in the case of 1.8 Ga

zircons, which are more significant in the oldest part of the sequence, where they are accompanied by a relatively high 2.5 Ga peak. This may suggest transport from the ILH unit. However, based on the Sr-Nd isotope record, the latter source is unlikely (see below). Moreover, the MDS analyses show a high level of dissimilarity between the ILH and the Siwalik sediments of the Subathu Basin (Figure 4). The dominant source of the detritus in the Upper Siwalik strata, we consequently associate with erosion of the HHCS. In the two top-most samples we see again the input of the young, Late Cretaceous–Cenozoic zircons. In sample USW 23-17, this young peak is accompanied by zircons typical of the HHCS, making the spectrum very similar to the LSW 9-10, which records sediment influx primarily from the THS and HHCS. The HHCS zircons are "underrepresented" in the USW 2-10 sample where the spectrum is dominated by just two peaks of 68 and 467 Ma. This makes it similar to the Middle Siwalik samples whose provenance was the Trans Himalayan Batholith with some contribution of the Ordovician granitoids frequently found in the Indian crust.

5.2 Provenance of The Cretaceous–Cenozoic Zircons

Our interpretation of the Cretaceous–Cenozoic zircons in the Subathu foreland basin presented above links them with the calc-alkaline Trans Himalayan Batholith intruding the southern Eurasian margin. Yet, the Cretaceous zircons are also found in the Stumpata Quartzite of the Zanskar region (Figure 1). In the Stumpata Quartzite, Cenozoic zircons are absent, and the Mesozoic population is limited to the age range 120–140 Ma (Clift et al., 2014). In our Siwalik samples, 120–140 Ma zircons are nearly absent (one grain), which excludes this formation as a potential source of the detritus. Alternatively, the Cretaceous zircons could be recycled from the volcaniclastic sandstones of the Pingdon La Formation of the Zankar Himalaya. The stratigraphic age of the Pingdon La Formation is inferred to be late Albian i.e. 113–100 Ma (Garzanti, 1992). However, the lack of zircon age data from this unit may only limit this argument to speculation. Even though we do find some zircons of this age range in our samples,

the main Cretaceous peaks in the Siwalik age spectra are some 20–30 Ma younger and accompanied by a range of Paleogene zircons. This points to a rather minor role, if any, of the Pingdong La Formation as sediment source for the Siwalik Group (Figures 3 and 5).

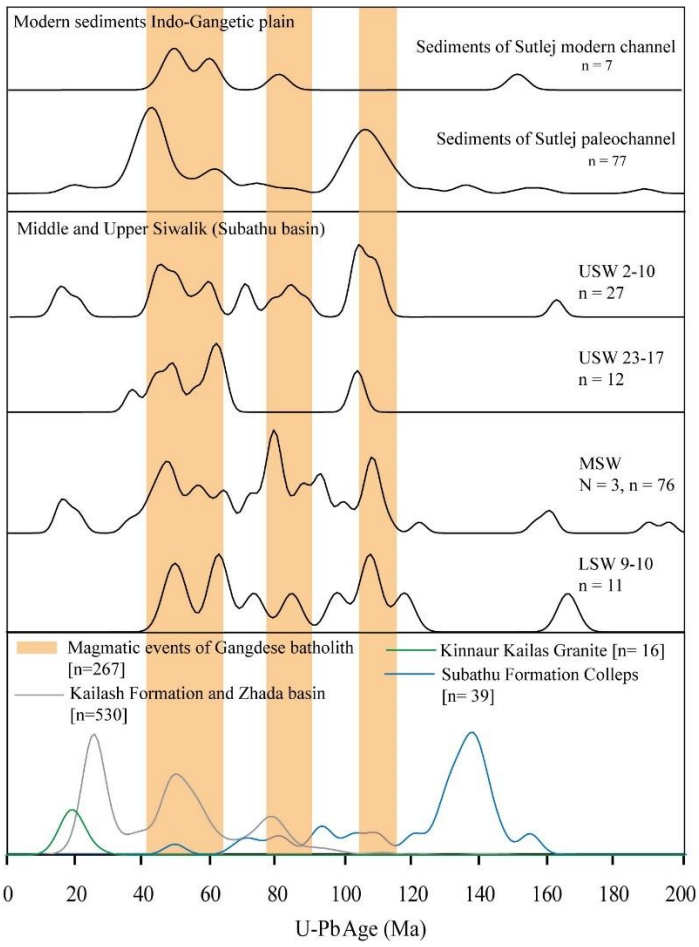

Figure 5. Comparison of the KDE spectra of the individual samples with <200 Ma zircons showing potential sources. Reference zircon spectra of the Gangdese Batholith compiled from Wang et al. (2012 and Zhang et al. (2011), Kailas Formation and Zhada Basin from DeCelles et al. (2011) and Saylor et al. (2010), and Subathu Formation from Colleps et al., 2020, 2019). The Miocene age of the Kinnaur Kailas granite of the HHCS in Himachal Pradesh is after Tripathi et al. (2012).

Reworking of the Subathu Formation can also be excluded as the primary source of the Cretaceous zircons, since this formation contains zircons significantly older (125–160 Ma, Colleps et al., 2020) than those defining the Cretaceous peak in the Siwalik sediments. Moreover, the Subathu Formation contains only very minor amount of the Paleogene zircons, which are frequent in the Siwalik samples (Figure 5). Hence, the most plausible source of the

youngest zircon age population are the granites of the Trans Himalayan Batholith. Timing of several magmatic pulses within the Transhimalayan Batholith, especially during the Paleogene, well correlates with the detrital zircon ages found in the Siwalik strata (DeCelles et al., 2011; Wang et al., 2012; Zhang et al., 2011) (Figure 5). All the Middle Siwalik samples and the Upper Siwalik sample USW 2-10 additionally show the presence of a small peak around 20 Ma (Figure 5). Zircons of this age are likely derived from the Miocene Kinnaur-Kailas leucogranite of the HHCS. Regardless of precise location of the source region, it is certainly located within the HHCS.

The presence of the Cretaceous–Paleogene zircons in the Neogene foreland basin of the NW Himalaya seems an exception rather than rule. They are absent in the neighboring Kangra Basin (Exnicios et al., 2022) as well as in the Dehradun region, about 100 km SE of the study area (Mandal et al., 2019). A simple explanation is that the Kangra Basin was supplied by the Beas River while the Dehradun was by mainly supplied by the Yamuna and its tributary rivers (Mandal et al., 2019) having no connection to the hinterland.

5.3 Sr-Nd-Hf Isotope Geochemistry

We compared bulk rock Sr-Nd-Hf isotopic composition with the values compiled from the potential source regions (Figure 7a, b). In general, the isotopic data support our inferences drawn from the detrital zircon dating. The results from the Kasauli Formation form a very coherent group with Sr-Nd composition indistinguishable from the broad range of values reported for the THS, HHCS and OLH (Figure 7a). The available Hf isotope database is still limited, but the Nd-Hf isotope systematics of the Kasauli Formation suggest a close affinity with the HHCS, however, they do not exclude some clastic supply from the THS (Figure 7b). Our observations are different from the previous studies of the Dharamsala Formation, equivalent of the Kasauli Formation in the adjoining Kangra Basin (Figure 1b), pointing to the HHCS as the only source area (Najman, 2006; White et al., 2002). This supports our

interpretation presented above indicating the Beas River drainage lacking connection to the hinterland, as the dominant sediment route to the Kangra Basin.

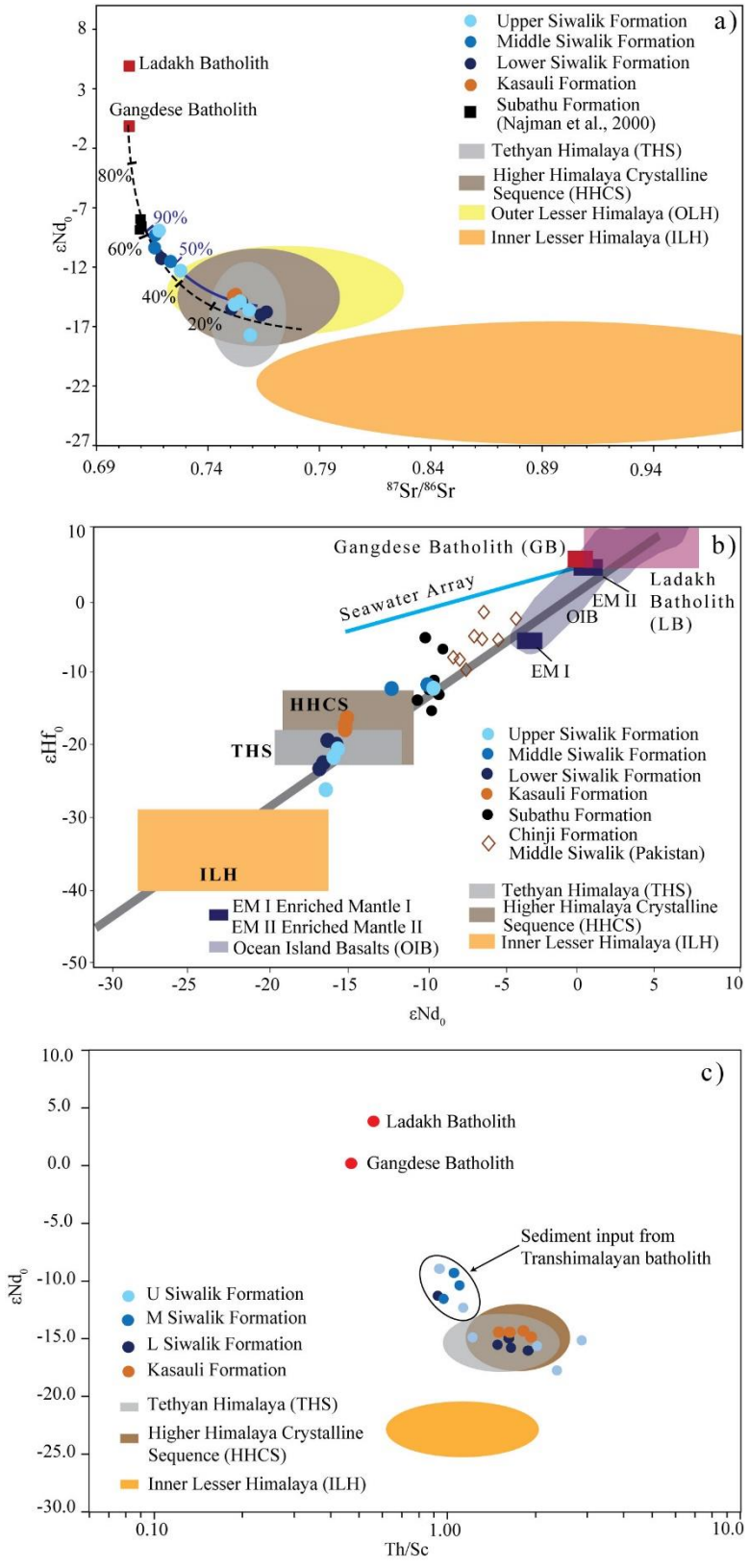

Figure 6. (**a**) εNd_0 vs $^{87}Sr/^{86}Sr$ diagram of the same samples compared to different source regions. The reference values of isotopes and Sr and Nd concentration of the THS, HHCS, OLH and ILH compiled from Mandal et al. (2019); for the Ladakh and Gangdese Batholith from Miller et al. (2000), Wang et al. (2015), Zhuang et al. (2015), Garçon et al. (2013) and Zhu et al. (2008); and for the Subathu Formation from Najman et al. (2000). The black dashed line is the mixing line between the Gangdese Batholith and HHCS. The solid blue line is the mixing line between the Subathu Formation and HHCS. (**b**) The εNd_0 vs εHf_0 plot shows that the foreland samples fall on the terrestrial array and show isotopic signature comparable that of the Higher Himalaya. Middle Siwalik samples and one Upper Siwalik sample plot close to the samples belonging to the Chinji Formation that is equivalent of the Middle Siwalik Formation in Pakistan (data from Chirouze et al., 2015). These samples show closer affinity to the Trans Himalayan Batholith (THB). Nd and Hf isotope data for the source regions including fluvial sediments from Nepal (pink field) are compiled from Garçon et al. (2013) and Zhuang et al. (2015). εNd_0 vs εHf_0 of mantle reservoirs are after Salters and White (1998). (**c**) Th/Sc vs εNd_0 plot (McLennan et al., 1993) of the Subathu foreland samples in comparison to the Himalayan and Trans Himalayan sources. Himalayan domains are shown as ellipses (values from Garçon et al., 2013) and the Trans Himalayan domains are shown as red circles (values from Bouilhol et al., 2013; Ma et al., 2013; Wang et al., 2015). The samples containing zircons potentially derived from the Ladakh and Gangdese arcs show Th/Sc values ≤ 1.

The Sr-Nd isotopic compositions of majority of the Siwalik Group rocks fall within the same field as the Kasauli sandstones (Figure 6a). The exceptions are samples containing the Cretaceous–Cenozoic zircons lying on a mixing line between the Trans Himalayan Batholith and the Indian crust domains (HHCS, THS and OLH). Part of the mixing curve includes the Subathu Formation, which opens the possibility that its reworking could have provided significant amounts of clastic detritus into younger increments. Modelling of the Sr-Nd bulk-rock isotope composition shows that about 40–90% of the Subathu Formation would have to be eroded away in order to provide sediments of the observed composition. Our zircon analyses presented above argue against such high participation of the reworked Subathu sediments in the Siwalik detritus. Thus, we favor an interpretation that the observed signature is the result of mixing between the detritus derived from the internal Himalaya and the Gangdese Batholith.

In the Nd-Hf isotope diagram, the Siwalik Group shows a similar pattern (Figure 6b). Majority of data plots along the terrestrial array with the Nd-Hf systematics closely resembling the HHCS and THS, which are very similar and, hence, it is difficult to distinguish these two sources. Samples containing the Late Cretaceous–Cenozoic component are much more

radiogenic and plot significantly above all remaining samples, near those from the Subathu Formation. We interpret this pattern as a mixture of the Gangdese Batholith-derived detritus with that supplied from different domains of the HHCS whose composition shows a very broad range.

Isotopes of Nd in conjunction with Th/Sc ratios were proved to be a useful source discriminator (McLennan et al., 1993). Indeed, present day εNd_0 vs Th/Sc plot defines two distinct groups of samples that correlate well with the discrimination based on detrital zircon geochronology. One group, with Th/Sc values ≤ 1.2 and $\varepsilon Nd_0 > -12.3$ correlates with the samples containing the Cretaceous–Cenozoic zircons derived from the Trans Himalaya, whereas the second group, with Th/Sc values >1.2 and $\varepsilon Nd_0 < -12.3$, represents typical THS and HHCS sources lacking the young zircons (Figure 6c).

5.4 Drainage Reorganization during the Miocene Exhumation of the Himalaya

The Neogene deposits of the Subathu Basin record uplift and exhumation history of the Indian NW Himalaya. A considerable increase in the sediment influx delivered to the foreland basin at the Oligocene–Miocene boundary (Figure 7a, b) is commonly linked to the initiation of the Main Central Thrust accommodating the rise of the HHCS (Grujic et al., 1996; Hodges et al., 1992; White et al., 2002). Not surprisingly, the sediments of that age represented by the Kasauli Formation were supplied primarily from the THS and HHCS constituting the highest part of the Himalayan range.

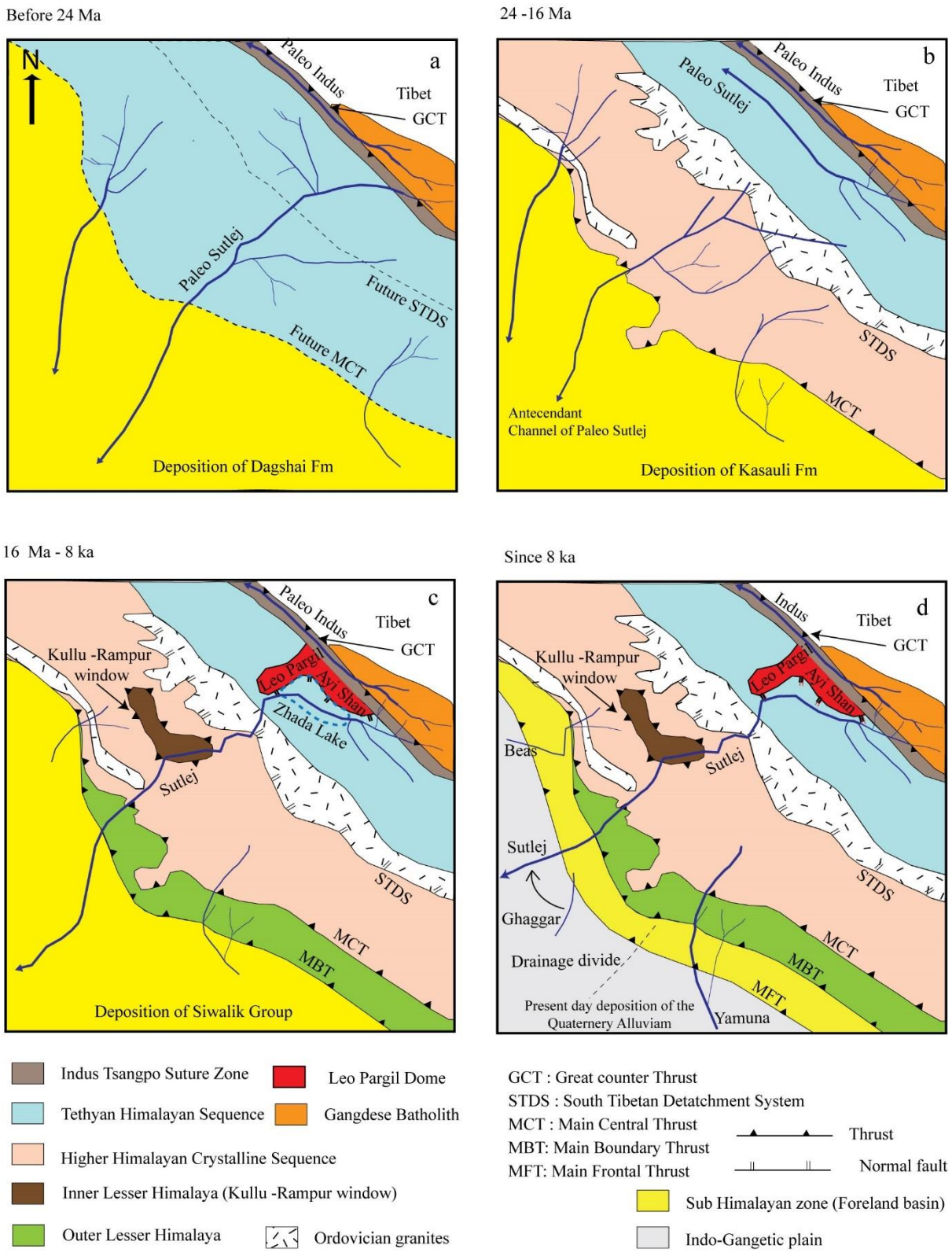

Figure 7. Schematic diagram of the inferred drainage reorganization of the Sutlej River since the latest Oligocene. (**a)** Before 24 Ma, the paleo-Sutlej flowed southwards from the Trans Himalayan Batholith across the Tethyan Himalayan Sequence to the Subathu Basin. (**b)** Between 24–16 Ma, the exhumation of the Higher Himalayan Sequence forced the paleo-Sutlej to a northwestward flow paralleling the course of the modern Indus River, whereas its cut-off channel may have turned into a separate river draining the HHS domain and having no connection to Trans Himalayan sources. (**c)** Since 16 Ma, the

exhumation of the Leo Pargil and Ayi Shan dome resulted in the damming of the paleo-Sutlej River and formation the Zhada lake (9 –1 Ma). This resulted in the capture of the Sutlej by its antecedent channel and the re-establishment of sediment routing across the Himalaya between the Transhimalaya and Subathu Basin. (**d**) At 8 ka, the Sutlej avulsed to its present course, leaving behind abandoned channels used by seasonal rivers like the Ghaggar that currently drains the study area.

The rapid uplift of the HHCS resulted in disconnecting the Sutlej source region from the foreland basin and directing its flow towards NW, along the strike of the Hiamlaya, (Figure 7b). The lower, antecedent part of the Sutlej River continued to drain the HHCS and THS (Figure 7b). This explains the absence of the Late Cretaceous–Paleogene zircons in the Kasauli Formation. Such physiographic configuration lasted until the beginning of the middle Miocene when the rapid uplift of the Leo Pargil and Ayi Shan domes took place (Thiede et al., 2006). The domes created a natural barrier for the Sutlej River, which diverted its course towards the SW and reconnected with its antecedent channel draining the Himalaya (Figure 7c). The presence of the Late Cretaceous–Paleogene zircons in some of the Lower Siwalik strata (13–11 Ma) indicates connection between the Trans Himalayan Batholith in the hinterland and the Subathu foreland basin. As argued earlier, the Gangdese Batholith seems the only plausible source of such young zircons. The rise of the domes led to the formation of an intramontane Zhada lake whose deposits also contain Cretaceous–Paleogene zircons (Saylor et al., 2010) supporting our inference about their hinterland provenance. Apatite fission track data show that the initial rapid uplift and exhumation of the Leo Pargil and Ayi Shan domes at about 16–14 Ma was followed by a period of slow cooling that lasted until ~4 Ma (Thiede et al., 2006). This period coincides with the deposition of the Middle Siwalik Formation (11–5 Ma), in which we observed the Gangdese batholith-derived zircons in all samples. We therefore conclude that this formation was fed primarily from Trans Himalayan sources, aided with a minor supply of zircons from the Higher Himalayan region (Figure 3a:7), and that the slower rate of uplift helped the Sutlej to maintain a more stable sediment transfer from the hinterland sources to the foreland basin at that time. In contrast, the Lower and Upper Siwalik formations show

fluctuating record of the Trans Himalayan detritus and this may reflect both tectonic and climatic forcing. Most of Himalayan rivers display monsoon-driven discharges that tend be low in the dry Tethyan Himalaya and increasing southeastwards when they become enhanced with monsoonal precipitation (Curray et al., 2002; Gabet et al., 2008; Lavé & Avouac, 2001). It seems likely that such discharge gradient was generally weaker during cold (dry) periods when the monsoon intensity decreases (Gebregiorgis et al., 2018) and this may have significantly reduced the Sutlej's transport capacity in its Trans Himalayan reaches. As a result of that increased influx from proximal HHCS source is observed in the provenance signals. The deposition of the Upper Siwalik Formation was accompanied by the renewed, rapid uplift and erosion of the HHCS as indicated by the AFT data (Thiede et al., 2004), as well as the exposure of the ILH in the Kulu-Rampur window (Figure 7c). The resultant catchment reorganization could have been instrumental in periodic damming and limiting or cutting-off sediment supply from the hinterland.

At 8 ka, the Sutlej River assumed its present course due to a drastic avulsion (A. Singh et al., 2017). The abandoned channel of the Sutlej is now used by the Ghaggar River, which drains mainly the Quaternary Indo-Gangetic Plain in the present-day Himalayan foreland basin west of the Subathu Basin (Figure 7d). The deposits of the modern Sutlej channel sampled in the Indo-Gangetic Plain just in front of the MFT reveal detrital zircon spectra typical of the HHCS with some addition of the ILH as suggested by the increased share of ~1.8 Ga zircons. As mentioned above, the Kulu-Rampur window, the largest exposure of the ILH, existed since ~2 Ma. Such timing well explains the absence of the ILH zircons in the studied Upper Siwalik Formation, whose deposition preceded this event. Our Upper Siwalik samples almost certainly do not include such young deposits (≤2 Ma). Noteworthy, the modern Sutlej deposits still contain Paleogene zircons that can only be linked to the hinterland source or recycled foreland basin deposits. The absence of the Cretaceous zircons may reflect a small drainage

553 reorganization in the Ayilari and Kailas ranges, the Sutlej source region comprising the
554 Gangdese Batholith. It is also important to realize that Cretaceous magmatic component within
555 the Gangdese Batholith is volumetrically much smaller in comparison with Paleogene magmas.
556 Our interpretation is supported by zircon data from the youngest Sutlej paleo-channel deposits
557 investigated by Singh et al. (2017). Their KDE plot averaging deposits younger than 70 ka
558 clearly show a very strong ~105 Ma peak indicating that Cretaceous zircons may well still be
559 transported from the hinterland to the foreland basin (Figure 8). Nonetheless, Singh et al.
560 (2017) favor alternative sources, i.e., the Thar Desert and Indus alluvial plain, from which the
561 zircons arrived to the Indo-Gangetic Plain via aeolian transport. They argued that there is no
562 source in the Trans Himalayan domain to the east of the Ladakh-Kohistan arc that would yield
563 zircons of 40–100 Ma age range and, consequently, ruled out the Sutlej River as the delivery
564 route for the Trans Himalayan zircons. Our results contradict the latter interpretation.
565 Moreover, the Thar Desert originated at 190–60 ka (Dhir et al., 2010; Singhvi et al., 2010;
566 Singhvi & Kar, 2004) and hence could not supply detritus into the much older Subathu Basin
567 fill. We would argue that the Thar Desert was supplied with the Cretaceous zircons from the
568 Himalayan region by both the Sutlej and the Indus rivers.

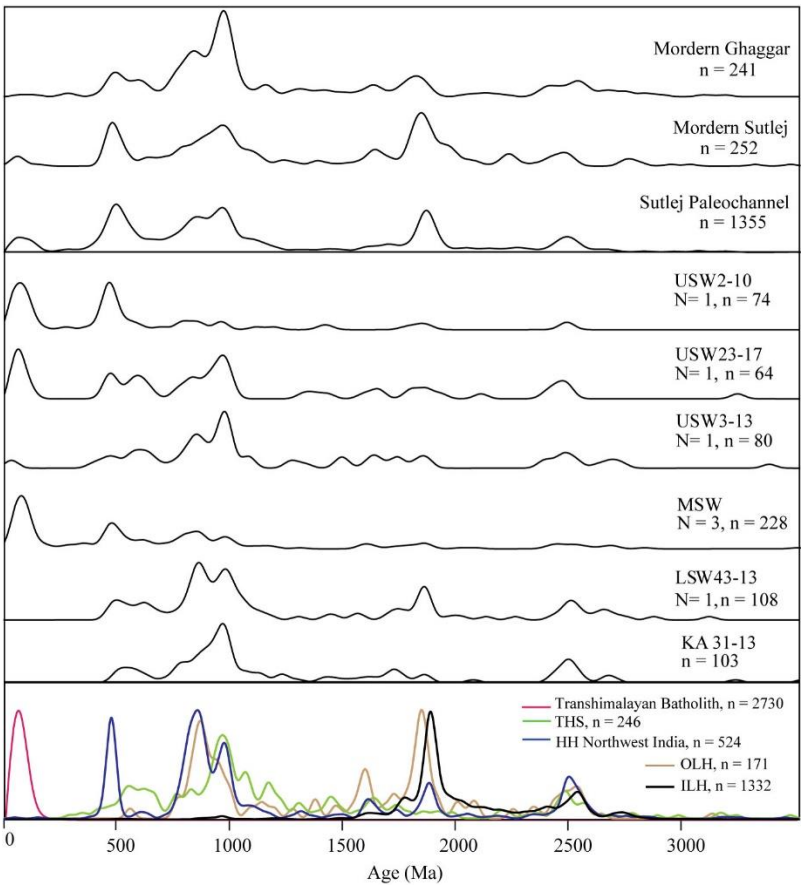

Figure 8 Comparison of the KDE of the zircon spectra of the Kasauli Formation and the Siwalik Group (this study) with the modern Sutlej and Ghaggar rivers and Sutlej paleochannel deposits (Alizai et al., 2011; Singh et al., 2017). Reference spectra are described in caption to Figure 3b.

6 Conclusions

Detrital zircon geochronology and isotopic proxies point to three major source areas of the Kasauli Formation and Siwalik Group sediments in the Subathu Basin belonging to the Himalayan foreland basin system. These are the Tethyan Himalayan Sequence, Higher Himalayan Crystalline Sequence, and Gangdese Batholith in the Trans Himalaya. The Kasauli Formation received clastic detritus dominantly from the THS and HHCS. The Lower Siwalik Formation was mainly sourced from the HHCS and, occasionally, from the Gangdese Batholith. The Middle Siwalik Formation records contribution dominantly from the Trans Himalayan domain and the Ordovician granitoids of the HHCS. The Upper Siwalik Formation

584 shows major inputs from the HHCS and the Trans Himalaya. The fingerprint of the Gangdese
585 Batholith is the Late Cretaceous (110–80 Ma) detrital-zircon population.

586 The recurrence of the Late Cretaceous–Cenozoic zircons throughout the Subathu Basin infill
587 points to the episodic transport from the Trans Himalayan Gangdese batholithic source. We
588 postulate that the Sutlej River linked the Subathu foreland basin with the hinterland sources.
589 During the deposition of the Kasauli and Lower Siwalik formations, the rapid uplift of the
590 HHCS diverted the Sutlej to flow north-westerly parallel to the orogen which cut-off the
591 sediment supply from the Trans Himalaya to the foreland basin. Subsequently, the rise of the
592 Leo Pargil dome during the middle Miocene diverted the Sutlej back to its earlier antecedent
593 channel across the rising Himalaya. This resulted in the re-establishing sediment routing system
594 between the hinterland and the foreland basin. The small-scale fluctuations in the presence of
595 the Trans Himalayan zircons observed in the Lower and Upper Siwalik formations may reflect
596 climatic forcing associated with changing monsoon precipitation and the Sutlej's capacity of
597 transporting fluvial load for long distance between cold (dry) and warm (moist) cycles.

598

599 **Acknowledgments**

600 We thank Dariusz Sala, Marta Smędra and Milena Matyszczak for assistance during ultraclean
601 chemistry work and LA-ICPMS analyses. We also thank Anna Zagórska, Izabela Kocjan and
602 Tomasz Siwecki for sample preparation and Vijay Kumar for logistic support during fieldwork.
603 This research was funded by NCN grant No. 2015/17/N/ST10/03137 awarded to Akeek Maitra.

604 **Open Research**

605 The results presented in this study will be available in EPOS^{PL+} database via
606 https://database.ing.pan.pl/

References

Alizai, A., Carter, A., Clift, P. D., VanLaningham, S., Williams, J. C., & Kumar, R. (2011). Sediment provenance, reworking and transport processes in the Indus River by U-Pb dating of detrital zircon grains. *Global and Planetary Change*, *76*(1–2), 33–55. https://doi.org/10.1016/j.gloplacha.2010.11.008

Allen, P. A. (2017). *Sediment Routing Systems: The Fate of Sediment from Source to Sink*. Cambridge: Cambridge University Press. https://doi.org/DOI: 10.1017/9781316135754

Anczkiewicz, A. A., & Anczkiewicz, R. (2016). U-Pb zircon geochronology and anomalous Sr-Nd-Hf isotope systematics of late orogenic andesites: Pieniny Klippen Belt, Western Carpathians, South Poland. *Chemical Geology*, *427*(February), 1–16. https://doi.org/10.1016/j.chemgeo.2016.02.004

Arya, R, Ambwani, K., Sahni, N., & Sahni, A. (2004). First mammal and additional fossil flowers from the Kasauli Formation, Kasauli, Himachal Pradesh. *Journal-Geological Society of India*, *64*, 317–324.

Arya, Ritesh, & Awasthi, N. (1994). A new species of Bauhinia from the Kasauli Formation (Lower Miocene), Kasauli, Himachal Pradesh. *Geophytology*, *24*(1), 59–62.

Arya, Ritesh, Guleria, J. S., & Srivastava, R. (2001). New records of plant fossils from the Kasauli sediments of Himachal Pradesh, north-west India. *Phytomorphology*, *51*(1), 63–69.

Awasthi, N., Guleria, J. S., Prasad, M., & Srivastava, R. (1994). Occurrence of Acrostichum Linn., a coastal fern in the Tertiary sediments of Kasauli, Himachal Pradesh, north-west Himalaya. *Palaeobotanist 43*(2), 83-87

Bard, J. P. (1983). Metamorphism of an obducted island arc: Example of the Kohistan sequence (Pakistan) in the Himalayan collided range. *Earth and Planetary Science Letters*, *65*(1), 133–144. https://doi.org/10.1016/0012-821X(83)90195-4

Beaumont, C. (1981). Foreland basins. *Geophysical Journal International*, *65*(2), 291–329. https://doi.org/10.1111/J.1365-246X.1981.TB02715.X

Bera, M. K., Sarkar, A., Chakraborty, P. P., Loyal, R. S., & Sanyal, P. (2008). Marine to continental transition in Himalayan foreland. *Bulletin of the Geological Society of America*, *120*(9–10), 1214–1232. https://doi.org/10.1130/B26265.1

Bera, M. K., Sarkar, A., Chakraborty, P. P., Ravikant, V., & Choudhury, A. K. (2010). Forced regressive shoreface sandstone from Himalayan foreland: Implications to early Himalayan tectonic evolution. *Sedimentary Geology*, *229*(4), 268–281.

Bhatia, S. B., & Bhargava, O. N. (2006). Biochronological continuity of the Paleogene sediments of the Himalayan Foreland Basin: paleontological and other evidences. *Journal of Asian Earth Sciences 26*(5), 477-487. https://doi.org/10.1016/j.jseaes.2004.10.007

644 Bishop, M. P., Shroder Jr, J. F., Bonk, R., & Olsenholler, J. (2002). Geomorphic change in
645 high mountains: a western Himalayan perspective. *Global and Planetary Change*, *32*(4),
646 311–329.

647 Blum, M., Rogers, K., Gleason, J., Najman, Y., Cruz, J., & Fox, L. (2018). Allogenic and
648 Autogenic Signals in the Stratigraphic Record of the Deep-Sea Bengal Fan. *Scientific*
649 *Reports 8*(7973), 1–13. https://doi.org/10.1038/s41598-018-25819-5

650 Bosch, D., Garrido, C. J., Bruguier, O., Dhuime, B., Bodinier, J. L., Padròn-Navarta, J. A., &
651 Galland, B. (2011). Building an island-arc crustal section: Time constraints from a LA-
652 ICP-MS zircon study. *Earth and Planetary Science Letters*, *309*(3–4), 268–279.
653 https://doi.org/10.1016/j.epsl.2011.07.016

654 Bouilhol, P., Jagoutz, O., Hanchar, J. M., & Dudas, F. O. (2013). Dating the India-Eurasia
655 collision through arc magmatic records. *Earth and Planetary Science Letters*, *366*, 163–
656 175. https://doi.org/10.1016/j.epsl.2013.01.023

657 Bouvier, A., Vervoort, J. D., & Patchett, P. J. (2008). The Lu-Hf and Sm-Nd isotopic
658 composition of CHUR: Constraints from unequilibrated chondrites and implications for
659 the bulk composition of terrestrial planets. *Earth and Planetary Science Letters*, *273*(1–
660 2), 48–57. https://doi.org/10.1016/j.epsl.2008.06.010

661 Bracciali, L., Najman, Y., Parrish, R. R., Akhter, S. H., & Millar, I. (2015). The Brahmaputra
662 tale of tectonics and erosion: Early Miocene river capture in the Eastern Himalaya.
663 *Earth and Planetary Science Letters*, *415*(January 2016), 25–37.
664 https://doi.org/10.1016/j.epsl.2015.01.022

665 Brozovic, N., & Burbank, D. W. (2000). Dynamic fluvial systems and gravel progradation in
666 the Himalayan foreland. *GSA Bulletin*, *112*(3), 394–412.

667 Burbank, D. W., Beck, R. A., Mulder, T., Yin, A., & Harrison, T. M. (1996). The Himalayan
668 foreland basin. *World and Regional Geology*, 149–190.

669 Burg, J. P., & Chen, G. M. (1984). Tectonics and structural zonation of southern Tibet,
670 China. *Nature*, *311*(5983), 219–223.

671 Cawood, P. A., Nemchin, A. A., & Strachan, R. (2007). Provenance record of Laurentian
672 passive-margin strata in the northern Caledonides: Implications for paleodrainage and
673 paleogeography. *Bulletin of the Geological Society of America*, *119*(7–8), 993–1003.
674 https://doi.org/10.1130/B26152.1

675 Chirouze, F., Huyghe, P., Chauvel, C., van der Beek, P., Bernet, M., & Mugnier, J. L. (2015).
676 Stable drainage pattern and variable exhumation in the western himalaya since the
677 middle miocene. *Journal of Geology*, *123*(1), 1–20. https://doi.org/10.1086/679305

678 Clift, P D, Shimizu, N., Layne, G. D., Blusztajn, J. S., Gaedicke, C., Schlü, H.-U., et al.
679 (2001). Development of the Indus Fan and its significance for the erosional history of
680 the Western Himalaya and Karakoram. *Bulletin of the Geological Society of America*,
681 *113*(8), 1039-1051. https://doi.org/10.1130/0016-
682 7606(2001)113<1039:DOTIFA>2.0.CO;2

683 Clift, Peter D., & Blusztajn, J. (2005). Reorganization of the western Himalayan river system
684 after five million years ago. *Nature*, *438*(7070), 1001–1003.
685 https://doi.org/10.1038/nature04379

686 Clift, Peter D., Carter, A., & Jonell, T. N. (2014). U-Pb dating of detrital zircon grains in the
687 Paleocene Stumpata Formation, Tethyan Himalaya, Zanskar, India. *Journal of Asian*
688 *Earth Sciences*, *82*, 80–89. https://doi.org/10.1016/j.jseaes.2013.12.014

689 Colleps, C. L., Stockli, D. F., McKenzie, N. R., Webb, A. A. G., & Horton, B. K. (2019).
690 Neogene Kinematic Evolution and Exhumation of the NW India Himalaya: Zircon Geo-
691 and Thermochronometric Insights From the Fold-Thrust Belt and Foreland Basin.
692 *Tectonics*, *38*(6), 2059–2086. https://doi.org/10.1029/2018TC005304

693 Colleps, C. L., McKenzie, N. R., Horton, B. K., Webb, A. A. G., Ng, Y. W., & Singh, B. P.
694 (2020). Sediment provenance of pre- and post-collisional Cretaceous–Paleogene strata
695 from the frontal Himalaya of northwest India. *Earth and Planetary Science Letters*, *534*.
696 https://doi.org/10.1016/j.epsl.2020.116079

697 Curray, J. R., Emmel, F. J., & Moore, D. G. (2002). The Bengal Fan: morphology, geometry,
698 stratigraphy, history and processes. *Marine and Petroleum Geology*, *19*(10), 1191–1223.
699 https://doi.org/10.1016/S0264-8172(03)00035-7

700 DeCelles, P. G., Kapp, P., Quade, J., & Gehrels, G. E. (2011). Oligocene-Miocene Kailas
701 basin, southwestern Tibet: Record of postcollisional upper-plate extension in the Indus-
702 Yarlung suture zone. *Bulletin of the Geological Society of America*, *123*(7–8), 1337–
703 1362. https://doi.org/10.1130/B30258.1

704 DeCelles, P. G., & Giles, K. A., (1996). Foreland basin systems. *Basin Research*, *8*(2), 105–
705 123.

706 DeCelles, Peter G., Gehrels, G. E., Quade, J., & Ojha, T. P. (1998). Eocene-early Miocene
707 foreland basin development and the history of Himalayan thrusting, western and central
708 Nepal. *Tectonics*, *17*(5), 741–765. https://doi.org/10.1029/98TC02598

709 Dhir, R. P., Singhvi, A. K., Andrews, J. E., Kar, A., Sareen, B. K., Tandon, S. K., et al.
710 (2010). Multiple episodes of aggradation and calcrete formation in Late Quaternary
711 aeolian sands, Central Thar Desert, Rajasthan, India. *Journal of Asian Earth Sciences*,
712 *37*(1), 10–16. https://doi.org/10.1016/j.jseaes.2009.07.002

713 Dubille, M., & Lavé, J. (2015). Rapid grain size coarsening at sandstone/conglomerate
714 transition: Similar expression in Himalayan modern rivers and Pliocene molasse
715 deposits. *Basin Research*, *27*(1), 26–42. https://doi.org/10.1111/BRE.12071

716 Eisbacher, G. H., Carrigy, M. A., & Campbell, R. B. (1974). Paleodrainage Pattern and Late-
717 Orogenic Basins of the Canadian Cordillera. In Dickinson, W.R., (Ed) *Tectonics and*
718 *Sedimentation 22,* 143–166. https://doi.org/10.2110/pec.74.22.0143

719 Exnicios, E. M., Carter, A., Najman, Y., & Clift, P. D. (2022). Late Miocene unroofing of the
720 Inner Lesser Himalaya recorded in the NW Himalaya foreland basin. *Basin Research*,
721 *34*(6), 1894–1916. https://doi.org/10.1111/BRE.12689

Le Fort, P. (1988). Granites in the tectonic evolution of the Himalaya, Karakoram and southern Tibet. *Philosophical Transactions of the Royal Society of London. Series A, Mathematical and Physical Sciences*, *326*(1589), 281–299. https://doi.org/10.1098/RSTA.1988.0088

Gabet, E. J., Burbank, D. W., Pratt-Sitaula, B., Putkonen, J., & Bookhagen, B. (2008). Modern erosion rates in the High Himalayas of Nepal. *Earth and Planetary Science Letters*, *267*(3–4), 482–494. https://doi.org/10.1016/J.EPSL.2007.11.059

Garçon, M., Chauvel, C., France-Lanord, C., Huyghe, P., & Lavé, J. Ô. (2013). Continental sedimentary processes decouple Nd and Hf isotopes. *Geochimica et Cosmochimica Acta*, *121*, 177–195. https://doi.org/10.1016/j.gca.2013.07.027

Garzanti, E. (1992). Stratigraphy of the Early Cretaceous Giumal Group (Zanskar Range, Northern India). *Rivista Italiana Di Paleontologia e Stratigrafia*, *97*(3–4), 485-510.

Garzanti, Eduardo. (2019). The Himalayan Foreland Basin from collision onset to the present: a sedimentary–petrology perspective. *Geological Society, London, Special Publications*, *483*(1), 65–122.

Gebregiorgis, D., Hathorne, E. C., Giosan, L., Clemens, S., Nürnberg, D., & Frank, M. (2018). Southern Hemisphere forcing of South Asian monsoon precipitation over the past ~1 million years. *Nature Communications 2018 9:1*, *9*(1), 1–8. https://doi.org/10.1038/s41467-018-07076-2

Gehrels, G., Kapp, P., Decelles, P., Pullen, a., Blakey, R., Weislogel, a., et al. (2011). Detrital zircon geochronology of pre-Tertiary strata in the Tibetan-Himalayan orogen. *Tectonics*, *30*(5), TC5016. https://doi.org/10.1029/2011TC002868

Govin, G., Najman, Y., Dupont-Nivet, G., Millar, I., Van Der Beek, P., Huyghe, P., et al. (2018). The tectonics and paleo-drainage of the easternmost Himalaya (Arunachal Pradesh, India) recorded in the Siwalik rocks of the foreland basin. *American Journal of Science*, *318*(7), 764–798.

Grujic, D., Casey, M., Davidson, C., Hollister, L. S., Kündig, R., Pavlis, T., & Schmid, S. (1996). Ductile extrusion of the Higher Himalayan Crystalline in Bhutan: evidence from quartz microfabrics. *Tectonophysics*, *260*(1–3), 21–43. https://doi.org/10.1016/0040-1951(96)00074-1

Grujic, D., Coutand, I., Bookhagen, B., Bonnet, S., Blythe, A., & Duncan, C. (2006). Climatic forcing of erosion, landscape, and tectonics in the Bhutan Himalayas. *Geology*, *34*(10), 801–804. https://doi.org/10.1130/G22648.1

Hamilton, P. J., O'Nions, R. K., Bridgwater, D., & Nutman, A. (1983). Sm-Nd studies of Archaean metasediments and metavolcanics from West Greenland and their implications for the Earth's early history. *Earth and Planetary Science Letters*, *62*(2), 263–272. https://doi.org/10.1016/0012-821X(83)90089-4

Hirst, J. P. P., & Nichols, G. J. (1986). Thrust tectonic controls on Miocene alluvial distribution patterns, southern Pyrenees. *Foreland Basins*, 247–258. https://doi.org/10.1002/9781444303810.ch13

Hodges, K. V., Parrish, R. R., Housh, T. B., Lux, D. R., Burchfiel, B. C., Royden, L. H., & Chen, Z. (1992). Simultaneous miocene extension and shortening in the Himalayan orogen. *Science*, *258*(5087), 1466–1470. https://doi.org/10.1126/science.258.5087.1466

Horton, B. K., & Decelles, P. G. (2001). Modern and ancient fluvial megafans in the foreland basin system of the Central Andes, Southern Bolivia: Implications for drainage network evolution if foldthrust belts. *Basin Research*, *13*(1), 43–63. https://doi.org/10.1046/j.1365-2117.2001.00137.x

Huntington, K. W., Blythe, A. E., & Hodges, K. V. (2006). Climate change and Late Pliocene acceleration of erosion in the Himalaya. *Earth and Planetary Science Letters*, *252*(1–2), 107–118. https://doi.org/10.1016/j.epsl.2006.09.031

Jackson, S. E., Pearson, N. J., Griffin, W. L., & Belousova, E. A. (2004). The application of laser ablation-inductively coupled plasma-mass spectrometry to in situ U-Pb zircon geochronology. *Chemical Geology*, *211*(1–2), 47–69. https://doi.org/10.1016/j.chemgeo.2004.06.017

Jacobsen, S. B., & Wasserburg, G. J. (1980). Sm-Nd isotopic evolution of chondrites. *Earth and Planetary Science Letters*, *50*(1), 139–155. https://doi.org/10.1016/0012-821X(80)90125-9

Jagoutz, O. E., Burg, J. P., Hussain, S., Dawood, H., Pettke, T., Iizuka, T., & Maruyama, S. (2009). Construction of the granitoid crust of an island arc part I: Geochronological and geochemical constraints from the plutonic Kohistan (NW Pakistan). *Contributions to Mineralogy and Petrology*, *158*(6), 739–755. https://doi.org/10.1007/s00410-009-0408-3

Jain, A. K., Lal, N., Sulemani, B., Awasthi, A. K., Singh, S., Kumar, R., & Kumar, D. (2009). Detrital-zircon fission-track ages from the Lower Cenozoic sediments, NW Himalayan foreland basin: Clues for exhumation and denudation of the Himalaya during the India-Asia collision. *Geological Society of America Bulletin*, *121*(3–4), 519–535.

Jordan, T. E. (1981). Thrust Loads and Foreland Basin Evolution, Cretaceous, Western United States. *AAPG Bulletin*, *65*(12), 2506–2520. https://doi.org/10.1306/03B599F4-16D1-11D7-8645000102C1865D

Khan, A. U., & Prasad, S. (1998). Geological quadrangle map 53F. *Geological Survey of India*.

Khan, M. A., Stern, R. J., Gribble, R. F., & Windley, B. F. (1997). Geochemical and isotopic constraints on subduction polarity, magma sources, and palaeogeography of the Kohistan intra-oceanic arc, northern Pakistan Himalaya. *Journal of the Geological Society*, *154*(6), 935–946. https://doi.org/10.1144/GSJGS.154.6.0935

Koshnaw, R. I., Horton, B. K., Stockli, D. F., Barber, D. E., Tamar-Agha, M. Y., & Kendall, J. J. (2017). Neogene shortening and exhumation of the Zagros fold-thrust belt and foreland basin in the Kurdistan region of northern Iraq. *Tectonophysics*, *694*, 332–355. https://doi.org/10.1016/J.TECTO.2016.11.016

Krol, M. A., Zeitler, P. K., & Copeland, P. (1996). Episodic unroofing of the Kohistan Batholith, Pakistan: Implications from K-feldspar thermochronology. *Journal of*

Geophysical Research: Solid Earth, *101*(B12), 28149–28164. https://doi.org/10.1029/96JB01503

Lavé, J., & Avouac, J. P. (2001). Fluvial incision and tectonic uplift across the Himalayas of central Nepal. *Journal of Geophysical Research: Solid Earth*, *106*(B11), 26561–26591. https://doi.org/10.1029/2001jb000359

Leonard, J. S., Fosdick, J. C., & VanderLeest, R. A. (2020). Erosional and Tectonic Evolution of a Retroarc Orogenic Wedge as Revealed by Sedimentary Provenance: Case of the Oligocene – Miocene Patagonian Andes. *Frontiers in Earth Science*, *7*, 492057. https://doi.org/10.3389/FEART.2019.00353/BIBTEX

Lugmair, G. W., & Marti, K. (1978). Lunar initial 143Nd/144Nd: Differential evolution of the lunar crust and mantle. *Earth and Planetary Science Letters*, *39*(3), 349–357. https://doi.org/10.1016/0012-821X(78)90021-3

Maitra, A., Anczkiewicz, A. A., Anczkiewicz, R., Dunkl, I., & Mukhopadhyay, D. K. (2021). Thrusting sequence in the Western Himalayan foreland basin during the late phase of continental collision defined by low-temperature thermochronology. *Tectonophysics*, *821*, 229145. https://doi.org/10.1016/J.TECTO.2021.229145

Mandal, S., Robinson, D. M., Khanal, S., & Das, O. (2015). Redefining the tectonostratigraphic and structural architecture of the Almora klippe and the Ramgarh-Munsiari thrust sheet in NW India. In *Geological Society Special Publication* (Vol. 412, pp. 247–269). Geological Society of London. https://doi.org/10.1144/SP412.6

Mandal, S. K., Scherler, D., Romer, R. L., Burg, J. P., Guillong, M., & Schleicher, A. M. (2019). Multiproxy Isotopic and Geochemical Analysis of the Siwalik Sediments in NW India: Implication for the Late Cenozoic Tectonic Evolution of the Himalaya. *Tectonics*, *38*(1), 120–143. https://doi.org/10.1029/2018TC005200

McLennan, S. M., Hemming, S., McDaniel, D. K., & Hanson, G. N. (1993). Geochemical approaches to sedimentation, provenance, and tectonics. *Geololgical Society of America-Special Paper*, *284*, 21–40.

Meigs, A. J., Burbank, D. W., & Beck, R. A. (1995). Middle-late Miocene (> 10 Ma) formation of the Main Boundary thrust in the western Himalaya. *Geology*, *23*(5), 423–426.

Miller, C., Klötzli, U., Frank, W., Thöni, M., & Grasemann, B. (2000). Proterozoic crustal evolution in the NW Himalaya (India) as recorded by circa 1.80 Ga mafic and 1.84 Ga granitic magmatism. *Precambrian Research*, *103*(3–4), 191–206. https://doi.org/10.1016/S0301-9268(00)00091-7

Mishra, P., & Mukhopadhyay, D. K. (2012). Structural evolution of the frontal fold–thrust belt, NW Himalayas from sequential restoration of balanced cross-sections and its hydrocarbon potential. *Geological Society, London, Special Publications*, *366*(1), 201–228.

Myrow, P. M., Hughes, N. C., Goodge, J. W., Fanning, C. M., Williams, I. S., Peng, S., et al. (2010). Extraordinary transport and mixing of sediment across Himalayan central

Gondwana during the Cambrian–Ordovician. *GSA Bulletin*, *122*(9–10), 1660–1670. https://doi.org/10.1130/B30123.1

Najman, Bickle, Chapman, & Yang, H. (2000). Early Himalayan exhumation: Isotopic constraints from the Indian foreland basin. *Terra Nova*, *12*(1), 28–34. https://doi.org/10.1046/j.1365-3121.2000.00268.x

Najman, Y., & Garzanti, E. (2000). Reconstructing early Himalayan tectonic evolution and paleogeography from Tertiary foreland basin sedimentary rocks, northern India. *Bulletin of the Geological Society of America*, *112*(3), 435–449. https://doi.org/10.1130/0016-7606(2000)112<435:REHTEA>2.0.CO;2

Najman, Y. M. R., Pringle, M. S., Johnson, M. R. W., Robertson, A. H. F., & Wijbrans, J. R. (1997). Laser 40Ar/39Ar dating of single detrital muscovite grains from early foreland-basin sedimentary deposits in India: Implications for early Himalayan evolution. *Geology*, *25*(6), 535–538. https://doi.org/10.1130/0091-7613(1997)025<0535:LAADOS>2.3.CO;2

Najman, Y., (2006). The detrital record of orogensis: A review of approaches and techniques used in the Himalayan sedimentary basins. *Earth-Science Reviews*, *74*(1–2), 1–72. https://doi.org/10.1016/j.earscirev.2005.04.004

Najman, Y., Johnson, C., White, N. M., Oliver, G., Johnson, K., White, N. M., (2004). Evolution of the Himalayan foreland basin, NW India. *Basin Research*, *16*(1), 1–24. https://doi.org/10.1111/j.1365-2117.2004.00223.x

Nanda, A. C. (2002). Upper Siwalik mammalian faunas of India and associated events. *Journal of Asian Earth Sciences*, *21*(1), 47–58.

Parkash, B., Sharma, R. P., & Roy, A. K. (1980). The Siwalik Group (molasse)—sediments shed by collision of continental plates. *Sedimentary Geology*, *25*(1–2), 127–159.

Patnaik, R. (2003). Reconstruction of Upper Siwalik palaeoecology and palaeoclimatology using microfossil palaeocommunities. *Palaeogeography, Palaeoclimatology, Palaeoecology*, *197*(1–2), 133–150.

Paton, C., Hellstrom, J., Paul, B., Woodhead, J., & Hergt, J. (2011). Iolite: Freeware for the visualisation and processing of mass spectrometric data. *Journal of Analytical Atomic Spectrometry*, *26*(12), 2508–2518.

Philip, G., Bhakuni, S. S., & Suresh, N. (2012). Late Pleistocene and Holocene large magnitude earthquakes along Himalayan Frontal Thrust in the central seismic gap in NW Himalaya, Kala Amb, India. *Tectonophysics*, *580*, 162–177.

Pilgrim, G E, & West, W. D. (1928). The structure and correlation of the of the Simla rocks: Geological Survey of India Memoirs, v. 53.

Pilgrim, Guy Elcock. (1910). *The geology of the Persian Gulf and the adjoining portions of Persia and Arabia*.

Pillans, B., Williams, M., Cameron, D., Patnaik, R., Hogarth, J., Sahni, A., et al. (2005). Revised correlation of the Haritalyangar magnetostratigraphy, Indian Siwaliks:

implications for the age of the Miocene hominids Indopithecus and Sivapithecus, with a note on a new hominid tooth. *Journal of Human Evolution*, *48*(5), 507–515.

Powers, P. M., Lillie, R. J., & Yeats, R. S. (1998). Structure and shortening of the Kangra and Dehra Dun reentrants, Sub-Himalaya, India. *Bulletin of the Geological Society of America*, *110*(8), 1010–1027. https://doi.org/10.1130/0016-7606(1998)110<1010:SASOTK>2.3.CO;2

Rao, A. R., Nanda, A. C., Sharma, U. N., & Bhalla, M. S. (1995). Magnetic polarity stratigraphy of the Pinjor Formation (Upper Siwalik) near Pinjore, Haryana. *Current Science*, 1231–1236.

Ravikant, V., Wu, F. Y., & Ji, W. Q. (2009). Zircon U-Pb and Hf isotopic constraints on petrogenesis of the Cretaceous-Tertiary granites in eastern Karakoram and Ladakh, India. *Lithos*, *110*(1–4), 153–166. https://doi.org/10.1016/j.lithos.2008.12.013

Ravikant, V., Wu, F. Y., & Ji, W. Q. (2011). U-Pb age and Hf isotopic constraints of detrital zircons from the Himalayan foreland Subathu sub-basin on the Tertiary palaeogeography of the Himalaya. *Earth and Planetary Science Letters*, *304*(3–4), 356–368. https://doi.org/10.1016/j.epsl.2011.02.009

Reynolds, P. H., Brookfield, M. E., & McNutt, R. H. (1983). The age and nature of Mesozoic-Tertiary magmatism across the Indus Suture Zone in Kashmir and Ladakh (N. W. India and Pakistan). *Geologische Rundschau*, *72*(3), 981–1003. https://doi.org/10.1007/BF01848351

Salters, V. J. M., & White, W. M. (1998). Hf isotope constraints on mantle evolution. *Chemical Geology*, *145*(3–4), 447–460. https://doi.org/10.1016/S0009-2541(97)00154-X

Saylor, J., DeCelles, P., Gehrels, G., Murphy, M., Zhang, R., & Kapp, P. (2010). Basin formation in the High Himalaya by arc-parallel extension and tectonic damming: Zhada basin, southwestern Tibet. *Tectonics*, *29*(1). https://doi.org/10.1029/2008TC002390

Schärer, U., Xu, R. H., & Allègre, C. J. (1984). UPb geochronology of Gangdese (Transhimalaya) plutonism in the Lhasa-Xigaze region, Tibet. *Earth and Planetary Science Letters*, *69*(2), 311–320. https://doi.org/10.1016/0012-821X(84)90190-0

Scherer, E., Münker, C., & Mezger, K. (2001). Calibration of the lutetium-hafnium clock. *Science*, *293*(5530), 683–687. https://doi.org/10.1126/science.1061372

Sehgal, R. K., & Bhandari, A. (2014). Miocene mammals from India: present status and future prospects. *Indian Miocene: A Geodynamic and Chronological Framework for Palaeobiota, Sedimentary Environments and Palaeoclimates. Palaeontol. Soc. India Spec. Publ*, *5*, 199–212.

Sharman, G. R., Sharman, J. P., & Sylvester, Z. (2018). detritalPy: A Python-based toolset for visualizing and analysing detrital geo-thermochronologic data. *The Depositional Record*, *4*(2), 202–215.

Singh, A., Thomsen, K. J., Sinha, R., Buylaert, J. P., Carter, A., Mark, D. F., et al. (2017). Counter-intuitive influence of Himalayan river morphodynamics on Indus Civilisation

urban settlements. *Nature Communications*, *8*(1617). https://doi.org/10.1038/s41467-017-01643-9

Singh, B. P. (2010). Marine to continental transition in Himalayan foreland: Discussion. *Bulletin of the Geological Society of America*, *122*(5-6), 954-955. https://doi.org/10.1130/B26532.1

Singh, I. B. (1978). On some sedimentological and palaeoecological aspects of Subathu-Dagshai-Kasauli succession of Simla Hills. *Journal of the Paleontological Society of India*, *21*, 19–28.

Singh, S., Kumar, R., Barley, M. E., & Jain, A. K. (2007). SHRIMP U-Pb ages and depth of emplacement of Ladakh Batholith, Eastern Ladakh, India. *Journal of Asian Earth Sciences*, *30*(3–4), 490–503. https://doi.org/10.1016/j.jseaes.2006.12.003

Singhvi, A. K., & Kar, A. (2004). The aeolian sedimentation record of the Thar desert. *Proceedings of the Indian Academy of Sciences, Earth and Planetary Sciences*, *113*(3), 371–401. https://doi.org/10.1007/BF02716733

Singhvi, A. K., Williams, M. A. J., Rajaguru, S. N., Misra, V. N., Chawla, S., Stokes, S., et al. (2010). A ~200 ka record of climatic change and dune activity in the Thar Desert, India. *Quaternary Science Reviews*, *29*(23–24), 3095–3105. https://doi.org/10.1016/j.quascirev.2010.08.003

Sláma, J., Košler, J., Condon, D. J., Crowley, J. L., Gerdes, A., Hanchar, J. M., et al. (2008). Plešovice zircon - A new natural reference material for U-Pb and Hf isotopic microanalysis. *Chemical Geology*, *249*(1–2), 1–35. https://doi.org/10.1016/j.chemgeo.2007.11.005

Spencer, C. J., Harris, R. A., & Dorais, M. J. (2012). Depositional provenance of the Himalayan metamorphic core of Garhwal region, India: Constrained by U-Pb and Hf isotopes in zircons. *Gondwana Research*, *22*(1), 26–35. https://doi.org/10.1016/j.gr.2011.10.004

Srivastava, G, Mehrotra, R. C., Shukla, A., & Tiwari, R. P. (2014). Miocene vegetation and climate in extra peninsular India: megafossil evidences. *Special Publication of the Palaeontological Society of India*, *5*, 283–290.

Srivastava, P., & Mitra, G. (1994). Thrust geometries and deep structure of the outer and lesser Himalaya, Kumaon and Garhwal (India): Implications for evolution of the Himalayan fold-and-thrust belt. *Tectonics*, *13*(1), 89–109.

St-Onge, M. R., Rayner, N., & Searle, M. P. (2010). Zircon age determinations for the Ladakh batholith at Chumathang (Northwest India): Implications for the age of the India-Asia collision in the Ladakh Himalaya. *Tectonophysics*, *495*(3–4), 171–183. https://doi.org/10.1016/j.tecto.2010.09.010

Tandon, S. K. (1991). The Himalayan Foreland: Focus on Siwalik Basin. *Sedimentary Basins of India. Tectonic Context*, 171–201. Retrieved from https://cir.nii.ac.jp/crid/1570572699294995200

960 Thiede, R. C., Bookhagen, B., Arrowsmith, J. R., Sobel, E. R., & Strecker, M. R. (2004).
961 Climatic control on rapid exhumation along the Southern Himalayan Front. *Earth and*
962 *Planetary Science Letters*, *222*(3–4), 791–806.

963 Thiede, R. C., Arrowsmith, J. R., Bookhagen, B., McWilliams, M., Sobel, E. R., & Strecker,
964 M. R. (2006). Dome formation and extension in the Tethyan Himalaya, Leo Pargil,
965 northwest India. *Bulletin of the Geological Society of America*, *118*(5–6), 635–650.
966 https://doi.org/10.1130/B25872.1

967 Tripathi, K., Sen, K., & Dubey, A. K. (2012). Modification of fabric in pre-Himalayan
968 granitic rocks by post-emplacement ductile deformation: Insights from microstructures,
969 AMS, and U-Pb geochronology of the Paleozoic Kinnaur Kailash Granite and associated
970 Cenozoic leucogranites of the South Tibetan. *International Journal of Earth Sciences*,
971 *101*(3), 761–772. https://doi.org/10.1007/s00531-011-0657-z

972 Upadhyay, R., Frisch, W., & Siebel, W. (2008). Tectonic implications of new U–Pb zircon
973 ages of the Ladakh batholith, Indus suture zone, northwest Himalaya, India. *Terra Nova*,
974 *20*(4), 309–317. https://doi.org/10.1111/j.1365-3121.2008.00822.x

975 Vermeesch, P. (2013). Multi-sample comparison of detrital age distributions. *Chemical*
976 *Geology*, *341*, 140–146. https://doi.org/10.1016/j.chemgeo.2013.01.010

977 Vermeesch, P. (2018). Dissimilarity measures in detrital geochronology. *Earth-Science*
978 *Reviews 178*, 310-321. https://doi.org/10.1016/j.earscirev.2017.11.027

979 Vermeesch, P., & Garzanti, E. (2015). Making geological sense of "Big Data" in sedimentary
980 provenance analysis. *Chemical Geology*, *409*, 20–27.
981 https://doi.org/10.1016/j.chemgeo.2015.05.004

982 Vezzoli, G., & Garzanti, E. (2009). Tracking paleodrainage in pleistocene foreland basins.
983 *Journal of Geology*, *117*(4), 445–454. https://doi.org/10.1086/598946

984 Wang, R., Richards, J. P., Hou, Z. qian, An, F., & Creaser, R. A. (2015). Zircon U-Pb age
985 and Sr-Nd-Hf-O isotope geochemistry of the Paleocene-Eocene igneous rocks in
986 western Gangdese: Evidence for the timing of Neo-Tethyan slab breakoff. *Lithos*, *224–*
987 *225*, 179–194. https://doi.org/10.1016/j.lithos.2015.03.003

988 Wang, S., Wang, C., Phillips, R. J., Murphy, M. A., Fang, X., & Yue, Y. (2012).
989 Displacement along the Karakoram fault, NW Himalaya, estimated from LA-ICP-MS
990 U-Pb dating of offset geologic markers. *Earth and Planetary Science Letters*, *337–338*,
991 156–163. https://doi.org/10.1016/j.epsl.2012.05.037

992 Webb, A. A. G., Yin, A., Harrison, T. M., Célérier, J., Gehrels, G. E., Manning, C. E., &
993 Grove, M. (2011). Cenozoic tectonic history of the Himachal Himalaya (northwestern
994 India) and its constraints on the formation mechanism of the Himalayan orogen.
995 *Geosphere*, *7*(4), 1013–1061. https://doi.org/10.1130/GES00627.1

996 White, L. T., Ahmad, T., Ireland, T. R., Lister, G. S., & Forster, M. A. (2011). Deconvolving
997 episodic age spectra from zircons of the Ladakh Batholith, northwest Indian Himalaya.
998 *Chemical Geology*, *289*(3–4), 179–196. https://doi.org/10.1016/j.chemgeo.2011.07.024

White, N. M., Parrish, R. R., Bickle, M. J., Najman, Y. M. R., Burbank, D., & Maithani, A. (2001). Metamorphism and exhumation of the NW Himalaya constrained by U–Th–Pb analyses of detrital monazite grains from early foreland basin sediments. *Journal of the Geological Society*, *158*(4), 625–635.

White, N. M., Pringle, M., Garzanti, E., Bickle, M., Najman, Y., Chapman, H., & Friend, P. (2002). Constraints on the exhumation and erosion of the High Himalayan Slab, NW India, from foreland basin deposits. *Earth and Planetary Science Letters*, *195*(1–2), 29–44.

Wu, F. Y., Clift, P. D., & Yang, J. H. (2007). Zircon Hf isotopic constraints on the sources of the Indus Molasse, Ladakh Himalaya, India. *Tectonics*, *26*(2), 1–15. https://doi.org/10.1029/2006TC002051

Yin, A. (2006). Cenozoic tectonic evolution of the Himalayan orogen as constrained by along-strike variation of structural geometry, exhumation history, and foreland sedimentation. *Earth-Science Reviews*, *76*(1–2), 1–131. https://doi.org/10.1016/j.earscirev.2005.05.004

Zhang, R., Murphy, M. A., Lapen, T. J., Sanchez, V., & Heizler, M. (2011). Late Eocene crustal thickening followed by Early-Late Oligocene extension along the India-Asia suture zone: Evidence for cyclicity in the Himalayan orogen. *Geosphere*, *7*(5), 1249–1268. https://doi.org/10.1130/GES00643.1

Zhuang, G., Najman, Y., Guillot, S., Roddaz, M., Antoine, P. O., Métais, G., et al. (2015). Constraints on the collision and the pre-collision tectonic configuration between India and Asia from detrital geochronology, thermochronology, and geochemistry studies in the lower Indus basin, Pakistan. *Earth and Planetary Science Letters*, *432*, 363–373. https://doi.org/10.1016/j.epsl.2015.10.026

Table 1. Whole rock Sr-Nd-Hf ratios of Kasauli Formation and Siwalik Group samples

Sample	Th/Sc	Rb [ppm]	Sr [ppm]	$^{87}Rb/^{86}Sr$	$^{87}Sr/^{86}Sr$	2 s.e	Sm [ppm]	Nd [ppm]	$^{147}Sm/^{144}Nd$	$^{143}Nd/^{144}Nd$	2 s.e	εNd_0	Lu [ppm]	Hf [ppm]	$^{176}Lu/^{177}Hf$	$^{176}Hf/^{177}Hf$	2 s.e	εHf_0
KA 19-17	1.82	60.3	48.20	3.6354	0.752525	0.000014	4.56	24.5	0.1125	0.511904	0.000005	-14.3	0.33	4.1	0.011	0.282330	0.000005	-16.1
KA 31-13	1.50	60.5	60.60	2.9010	0.751923	0.000012	4.1	21.9	0.1131	0.511898	0.000006	-14.4	0.4	4	0.014	0.282283	0.000004	-17.7
KA 33-16	1.63	56.3	42.30	3.8673	0.751317	0.000012	4.9	26.8	0.1105	0.511898	0.000004	-14.4	0.29	3.9	0.011	0.282302	0.000005	-17.1
KAS 2-10	1.93	61	31.20	5.6829	0.755084	0.000010	4.89	25.9	0.1141	0.511876	0.000015	-14.9	-	-		-	-	-
LSW 1-13	1.48	57.4	36.40	4.5816	0.750582	0.000012	3.73	19.5	0.1156	0.511843	0.000006	-15.5	0.28	4	0.010	0.282242	0.000004	-19.2
LSW 1-16	1.62	47.9	19.80	7.0318	0.755143	0.000011	4.32	21.4	0.1220	0.511871	0.000006	-15.0	0.26	3.9	0.010	0.282226	0.000005	-19.8
LSW 43-13	1.65	58.3	24.10	7.0391	0.766187	0.000012	3.86	20.8	0.1121	0.511829	0.000006	-15.8	0.31	5.1	0.009	0.282154	0.000006	-22.3
LSW 7-13	2.16	89.1	35.60	7.2810	0.763758	0.000011	5.72	31	0.1115	0.511817	0.000005	-16.0	0.38	8.9	0.006	0.282132	0.000006	-23.1
LSW 9-10	0.93	53.2	143.60	1.0731	0.719099	0.000012	4.53	23.9	0.1145	0.512060	0.000007	-11.3	-	-	-	-	-	-
MSW 5-13	0.97	71.6	137.40	1.5100	0.723234	0.000010	3.94	18.7	0.1273	0.512047	0.000005	-11.5	0.27	3	0.013	0.282443	0.000004	-12.1
MSW 6-13	1.05	53.8	180.20	0.8645	0.716359	0.000009	5.99	32.5	0.1114	0.512162	0.000005	-9.3	0.45	6.5	0.010	0.282459	0.000004	-11.5
MSW 5-10	1.10	45.4	212.80	0.6178	0.716043	0.000011	3.89	21.6	0.1088	0.512106	0.000012	-10.4	-	-	-	-	-	-
USW 6-10	2.37	58.2	71.60	2.3636	0.759001	0.000015	5.21	27.2	0.1157	0.511729	0.000008	-17.7	-	-	-	-	-	-
USW 3-13	2.70	36.3	18.70	5.6442	0.758382	0.000011	3.28	17.8	0.1113	0.511837	0.000006	-15.6	0.25	7.2	0.005	0.282051	0.000004	-26.0
USW 36-16	2.88	72	70.40	2.9718	0.751898	0.000011	4.43	23.6	0.1134	0.511862	0.000006	-15.1	0.3	6.1	0.007	0.282177	0.000007	-21.5
USW 4-13	1.53	40.5	22.90	5.1403	0.754423	0.000009	2.99	15.7	0.1151	0.511875	0.000007	-14.9	0.22	3.3	0.010	0.282209	0.000004	-20.4
USW 23-17	0.94	40.4	119.00	0.9832	0.718010	0.000016	2.27	11.9	0.1153	0.512180	0.000005	-8.9	0.16	1.8	0.013	0.282444	0.000005	-12.0
USW 2-10	1.28	75.9	88.70	2.4806	0.727683	0.000013	4.14	23.7	0.1055	0.512007	0.000021	-12.3	-	-	-	-	-	-

Uncertainties are expressed as 2SD (standard deviations). Reproducibility of Sr standard (SRM987) $^{87}Sr/^{86}Sr = 0.710265 \pm 0.000009$ (n = 6); Nd standard (JdNd-1) $^{143}Nd/^{144}Nd = 0.512103 \pm 0.000007$ (n=5) and Hf standard (JMC475) $^{176}Hf/^{177}Hf = 0.282156 \pm 0.000005$ (n=7) was achieved over a course of analyses. $^{143}Nd/^{144}NdCHUR(0) = 0.512638$ and $^{147}Sm/^{144}NdCHUR(0) = 0.0197$ (Hamilton et al., 1983; Jacobsen and Wasserburg, 1980); $^{176}Hf/^{177}HfCHUR(0) = 0.282785$ and 176Lu/177Hf CHUR(0) = 0.0336 (Bouvier et al., 2008). Decay constant $\lambda 147Sm = 6.54 \times 10^{-12}$ yr^{-1} (Lugmair and Marti, 1978). Decay constant $\lambda 176Lu = 1.865 \times 10^{-11}$ yr^{-1} adopted from (Scherer et al., 2001).